Stochastic Analysis Of Ground Response Variability Of The Seismic Design Of Buried Lifeline Structures

STOCHASTIC ANALYSIS OF GROUND RESPONSE VARIABILITY OF THE SEISMIC DESIGN OF BURIED LIFELINE STRUCTURES

T. Harada[1]

and

M. Shinozuka[2]

July 1986

1. Visiting Research Scientist, Columbia University; Associate Professor, Faculty of Engineering, Miyazaki University, Miyazaki, Japan.

2. Renwick Professor, Department of Civil Engineering and Engineering Mechanics, Columbia University, New York, NY.

ABSTRACT

Ground response variabilities in space and time, especially in space, have been analyzed using a stochastic ground surface model. The intent is to quantify the spatial variation of ground motions for the seismic analysis and design of buried lifeline structures such as gas or water supply pipelines. The ground is assumed to be composed of infinitely horizontal soil layers with stochastic soil thickness and soil properties which are supported on rigid base rock. The earthquake motion is subjected to the ground from rigid base rock with time lag x/c where x = horizontal coordinate and c = wave propagation speed in the x-direction. From this study, it is found that the spatial correlation function of the response displacement at the ground surface is a function of the response velocity spectrum, spatial correlation function of the predominant ground frequecy varying in the horizontal direction, the mean value of the quivalent damping ratio of the ground, the mean value of the predominant ground frequency, and the wave propagation speed in the horizontal direction.

1. INTRODUCTION

In contrast to the earthquake-resistant design of above-ground structures where intertial forces induced by ground acceleration are the main consideration, the spatial variation of the ground motion is of primary importance for buried lifeline structures such as pipelines and tunnels. Consistent with this observation, a response-displacement method was devised (Kubo et al., 1979) and is widelyused for the earthquake-resistant design of underground structures in Japan. However, the state-of-the-art of quantifying the spatial variability of earthquake ground motion and the permanent ground deformation resulting therefrom still leaves much to be desired.

It appears particularly important, now that dense array seismic data has begun to become available, to analyze the spatial variation of earthquake ground motions. In this context, several empirical studies are available from a direct statistical point of view (Loh et al., 1982; Vanmarcke and Harichandran, 1984; Harada, 1984; Harada and Shinozuka, 1986). The data on permanent ground deformation resulting from earthquakes has also been collected and analyzed from the statistical point of view (Harada et al., 1985). On the other hand, it is desirable to develop mechanistic models to study the ground motion problem from the analytical standpoint. Such models could be used not only to interpret seismic array data in terms of wave content but also as an aid in the development in site-specific earthquake-resistant design parameters. From this point of view, the spatial coherenece of earthquake ground motions has been studied using a stochastic model of SH waves travelling in homogeneous soil with varying angles (Kausel and Paris, 1984). The differential ground motions have been studied using sophisticated physical models of earthquake faulting (Bard and Bouchon, 1980; Zerva et al., 1985). From these last two studies, it is suggested, although expected empirically,

that the local soil condition is of relative importance for the spatial variabilities of ground motions.

In general, within the framework of wave propagation, the earthquake ground response variabilities in space as well as in time can be considered to result from numerous factors such as earthquake source characteristics and wave attenuation characteristics, dispersion and scattering characteristics affected by local soil conditions as well as site geology and stratification, etc. The relative importance of these factors depends on the representative spatial scale of the problem. For example, as suggested by the studies using physical models of earthquake faulting mentioned above, the scattering characteristics influenced by local soil conditions may not be neglected for differential ground motions within a few kilometers, whereas they are probablyless important then the wave attenuation characteristics at ten kilometers or more.

In this paper, the ground response variabilities in space and time, especially in space, have been analyzed using a stochastic ground surface model. The intent is to characterize the spatial variation of ground motions within a few kilometers where the spatial variation plays an important role in the seisic analysis and design of buried lifeline structures such as gas or water supply pipelines. In a conventional ground response analysis for earthquakes, it has been common to model the ground as soil layers with constant thickness and deterministic soil properties. However, under real ground conditions, the thickness and soil properties may vary erratically from point to point. Eventually this spatial stochasticity can be considered to affect the ground response variabilities not only in time but also in space. The stochastic model of ground resopnse variability developed i this paper incorporates not only the effect of the spatial variability of the soil thickness and soil properties but also the effect of wave propagation in the horizontal direction. The

ground is assumed to be composed of infinitely horizontal soil layers with stochastic properties, supported by rigid base rock. The earthquake motion is subjected to the stochastic ground from the rigid base rock with time lag x/c where x = horizontal coordinate and c = wave propagation speed in the x-direction.

2. HOMOGENEOUS STOCHASTIC HORIZONTAL GROUND MOTION

In a conventional ground response analysis, it is common to model the ground as layers with constant thickness and soil properties. However, in a real profile schematically shown in Fig. 1 where j denotes a typical soil layer and x and z measure the horizontal and vertical space coordinates, respectively, the soil thickness $H_j(x)$ of the j-th layer may vary randomly from point to point as a function of x. Similarly, the representative soil property q(x,z) may be a random function of x and z. In considering nominally or almost homogeneous horizontal soil layers as depicted in Fig. 1, it may be appropriate, at least for the first approximation, to assume that the soil thickness $H_j(x)$ and soil property q(x,z) are random functions only of the horizontal space coordinate x such that

$$H_j(x) = H_j[1 + f_{H_j}(x)] \tag{2.1a}$$

$$q(x,z) = q(z)[1 + f_q(x)] \tag{2.1b}$$

where H_j and q(z) are the expected values (mean values) of $H_j(x)$ and q(x,z) with respect to x, respectively, that is

$$E[H_j(x)] = H_j \text{ (constant)} \tag{2.2a}$$

$$E[q(x,z)] = q(z) \text{ (deterministic function of x)} \tag{2.2b}$$

Eventually, $f_{H_j}(x)$ and $f_q I.(x)$ in Eq. 1 represent the stochastic fluctuation of $H_j(x)$ and q(z,x) along the horizontal coordinate x with mean zero, $E[f_{H_j}(x)] = 0$ and $E[f_q(x)] = 0$.

It should be noted here that th term of almost homogeneous horizontal ground is relative depending on the scale of homogeneity of the ground, the scale of the representative distance of the problem, and the degree of accuracy required for the ground model. In fact, it is almost always possibvle to

reproduce homogeneous horizontal ground motion by considering the considerably long scale of representative distances (in both the horizontal and vertical directions) where entire buried valleys may appear as local variabilities in the homogeneous stochastic fields, but then the results from this model should be interpreted by taking into account the accuracy or sophistication of the model used in the analysis.

3. EQUATIONS OF MOTION FOR HOMOGENEOUS STOCHASTIC HORIZONTAL GROUND

3.1 Derivation of Equations of Motion

Consider homogeneous stochastic horizontal ground supported by rigid bedrock and subjected to earthquake ground motion as shown in Fig. 1. The total soil depth is assumed to be a constant H. The input earthquake ground motion is assumed to be a stationary random wave propagating with speed c in the x-direction and represented by

$$u_b(x,t) = u_b\left(t - \frac{x}{c}\right) \tag{3.1}$$

The relative displacement at the locations of x and z with respect to the input motion $u_b(x,t)$ at bedrock is denoted by $u^r(x,z,t)$.

Then the total response displacement u(x,z,t) can be expressed as

$$u(x,z,t) = u_b\left(t - \frac{x}{c}\right) + u^r(x,z,t) \tag{3.2}$$

By employing the generalized displacement concept (for example, Clough and Penzien, 1975), Eq. 3.2 can be written as

$$u(x,z,t) = u_b\left(t - \frac{x}{c}\right) + u^*(x,t)\psi(z) \tag{3.3}$$

where

$$u^r(x,z,t) = u^*(x,t)\psi(z) \tag{3.4a}$$

and

$$\psi(0) = 1 \tag{3.4b}$$

In Eqs. 3.3 and 3.4, $u^*(x,t)$ is the amplitude of motion or the generalized displacement and $\psi(z)$ is the given shape function or the assumed mode function. It is usually convenient, although not essential, to normalize the

shape function as given in Eq. 3.4b. The shape function must satisfy the geometric boundary conditions. When considering the ground at hand, the geometric boundary condition is given such that (see Fig. 1)

$$u^r(x,z,t) = 0 \qquad \text{at } z = H \tag{3.5}$$

The shape function can be arbitrarily assumed, provided it satisfies the geometric boundary conditions. However, it is better to assume a shape that can be expected to be similar to the deformation of the ground subjected to earthquake motion at bedrock. For simplicity in this paper, the shape function is assumed to be

$$\psi(z) = \cos\left(\frac{\pi z}{2H}\right) \tag{3.6}$$

The shape function in Eq. 3.6 corresponds to the first mode shape of a single homogeneous infinite horizontal layer lying on rigid bedrock (Clough and Penzien, 1975). Of course, Eq. 3.6 satisfies the geometric boundary conditions and the normalization given by Eqs. 3.4b and 3.5.

Under the conditions described above, consider the forces acting on a small soil element (dx x dz) within the ground as shown in Fig. 1. The inertial force F_I and restoring force F_R are given by

$$F_i = \rho(x,z)\ddot{u}^t(x,z,t)dxdz \tag{3.7}$$

$$F_R = k(x,z)u^r(x,z,t)dxdz \tag{3.8}$$

where $\ddot{u}^t(x,z,t) = \partial^2 u^t(x,z,t)/\partial t^2$ = the absolute acceleration of a soil particle at locations x and z, $\rho(x,z)$ = the soil mass per unit area at x and z, and $k(x,z)$ = the soil resistance per unit area at x and z. Recalling the definition of the homogeneous stochastic horizontal ground given in Eqs. 2.1 and 2.2, the soil mass and resistance can be expressed as

$$\rho(x,z) = \rho_z(z)[1 + f_\rho(x)] \tag{3.9}$$

$$k(x,z) = k_z(z)[1 + \rho_k(x)] \tag{3.10}$$

where $\rho_z(z)$ and $k_z(z)$ represent the means of $\rho(x,z)$ and $k(x,z)$ being the deterministic function of z. The functions $f_\rho(x)$ and $f_k(x)$ are random functions of the space coordinate x with zero means.

By utilizing the concept that the virtual work δW done by the virtual displacement δu^r is zero, that is

$$\delta W = \int_o^H (F_I + F_R)\delta u^r = 0 \tag{3.11}$$

where $\delta u^r = \psi(z)\delta u^*(x,t)$ since $\psi(z)$ is the given shape function, and substituting Eqs. 3.7 - 3.10 into Eq. 3.11, and introducing the equivalent damping ratio $h^*(x)$ to account for the vibration energy loss due to wave propagation as well as the hysteretic behavior of the soil stress-strain curve under dynamic loadings, one can obtain

$$\ddot{u}^*(x,t) + 2h^*(x)\omega^*(x)\dot{u}^*(x,t) + [\omega^*(x)]^2 u^*(x,t) = -\beta\ddot{u}_b\left(t - \frac{x}{c}\right) \tag{3.12}$$

where $\omega^*(x)$ = the ground natural circular frequency (rad/s) and β = the participation factor. They are given as

$$\div()x\text{-} = \sqrt{\frac{[1 + f_k(x)]\int_o^H k_z(z)\psi^2(z)dz}{[1 + f_\rho(x)]\int_o^H \rho_z(z)\psi^2(z)dz}} \tag{3.13}$$

$$\beta = \frac{\int_o^H \rho_z(z)\psi(z)dz}{\int_o^H \rho_z(z)\psi^2(z)dz} \tag{3.14}$$

3.2 Considerations for $\omega^*(x)$ and $h^*(x)$

Alternatively, for formal purposes, the (natural) predominant ground frequency $\omega^*(x)$ and the equivalent damping ratio $h^*(x)$ may also be expressed (as in Eq. 2.1) as

$$\omega^*(x) = \omega_0[1 + f(x)] \tag{3.15}$$

$$h^*(x) = h_0[1 + h(x)] \tag{3.16}$$

where ω_0 and h_0 are the means of $\omega^*(x)$ and $h^*(x)$, and $f(x)$ and $h(x)$ are homogeneous stochastic processes with zero means. In the present analysis, it is assumed that

$$|f(x)| << 1 \qquad \text{and} \qquad |h(x)| << 1 \tag{3.17}$$

For the expressions given in Eqs. 3.15 and 3.16, it is easy to show that

$$\delta_{\omega^*} = \sigma_{ff} \qquad \text{and} \quad \delta_{h^*} = \sigma_{hh} \tag{3.18}$$

where δ_{ω^*} and δ_{h^*} are the coefficients of variation of $\omega^*(x)$ and $h^*(x)$, respectively. And also, σ_{ff} and σ_{hh} are the standard deviations of $f(x)$ and $h(x)$, respectively.

For deterministic ground conditions where $f_k(x)$ and $f_\rho(x)$ can be considered to be zero in Eqs. 3.9 and 3.10, eventually $\omega^*(x) = \omega_0$ from Eq. 3.13, Okamoto (1984) empirically shows that the predominant ground frequency can be accurately estimated by:

$$\omega_0 = 2\pi f_0 = \frac{2\pi}{T_0} = \frac{2\pi}{4} \sum_{j=1}^{n} \frac{V_{sj}}{H_j} \tag{3.19}$$

where n = the total number of soil layers, f_0 = the predominant ground fre-

quency (Hz), T_0 = the predominant ground period (sec), H_j = the j-th later thickness and V_{sj} = the shear wave velocity of the j-th layer. Indeed, for its accuracy and simplicity, Eq. 3.19 has been adopted in the Seismic Design Guidelines for Highway Bridges in Japan (Japan Road Association, 1980).

In Eq.3.19, taking into account the horizontal variation of layer thickness $H_j(x)$ and the shear wave velocity $V_{sj}(x)$, then $\omega^*(x)$ may be expressed as

$$\omega^*(x) = 2\pi f^*(x) = \frac{2\pi}{T^*(x)} = \frac{2\pi}{4} \sum_{j=1}^{n} \frac{V_{sj}(x)}{H_j(x)} \tag{3.20}$$

Equation 3.20 is useful for the estimation of $\omega^*(x)$ from a set of ground data $H_j(x)$ and $V_{sj}(x)$. As is well known, although Eqs. 3.13 and 3.20 are suitable for the theoretical estimation of $\omega^*(x)$, the following alternative methods have also been utilized in the practice of estimation of predominant ground frequencies: (1) Measurement of microtremors, (2) observation of actual earthquakes, and (3) numerical simulation of ground response (Kanai, 1983; Okamoto, 1984).

Returning to the equivalent damping ratio $h^*(x)$, there still remains much uncertainty. For an elastic single soil layer $\left(f_k(x) = f_\rho(x) = 0\right)$ lying in a half-space layer, the equivalent damping ratio h_0 may be estimated by

$$h_0 = \frac{1}{2} \frac{\rho_1}{\rho_2} \frac{V_{s1}}{V_{s2}} \tag{3.21}$$

where ρ_j = the soil mass per unit area, and V_{sj} = the shear wave velocity (j = 1 for the surface later and 2 for the firm half-space). Equation 3.21 is derived in such a way that the maximum value of the transfer function for a single degree of freedom system is identical to that for an elastic surface layer lying in a half-space at the first (natural) frequency. For firm ground conditions, Tajimi (1964) suggests $h_0 = 0.6$ from the study of the shape of a

power spectral density function of earthquake ground acceleration. For relatively soft ground, as suggested from Eq. 3.21, the value of h_0 may become smaller than 0.6 since V_{s1} is small. For example, $h_0 = 0.08$ for $\rho_1 = \rho_2$, and $V_{s1} = 100$ m/s, $V_{s2} = 600$ m/s in Eq. 3.21. However, for soft ground, in addition to the energyloss due to wave propagation, the energy loss associated with the hysteretic behavior of the soil stress-strain curve must be taken into account. Unfortunately, at this time, no reliable results are available regarding the effect of material damping on the equivalent system (ground) damping ratio h_0 and hence no reliable estimation methods for $h^*(x)$ exist. However, this does not mean that the spatial (horizontal) variation of ground motion $u^t(x,z,t)$ obtained from the solution of Eq. 3.12 is not reliable, because the effect of damping $h^*(x)$ on the solution of Eq. 3.12 is considered to be the second factor compared with that of $\omega^*(x)$ at least for first-order approximations as described in a later section.

4. SPATIAL VARIABILITY OF GROUND MOTION RESPONSE

The solution of Eq. 3.12 is well known as

$$u^*(x,t) = -\beta \int_{-\infty}^{\infty} I(x,\tau)\ddot{u}_b\left(t - \tau - \frac{x}{c}\right)d\tau \qquad (4.1)$$

where $I(x,\tau)$ is the impulse response function given that

$$I(x,\tau) = \frac{1}{\omega^*(x)\sqrt{1 - [h^*(x)]^2}}\, e^{-h^*(x)\omega^*(x)\tau} \sin\left\{\omega^*(x)\sqrt{1 - [h^*(x)]^2}\,\tau\right\} \quad \text{for } \tau \geq 0$$

$$= 0 \quad \text{for } \tau < 0 \qquad (4.2)$$

Substituting Eq. 4.1 into Eq. 3.3, the total ground response $u(x,z,t)$ can be obtained. For the ground surface displacement response ($z = 0$), recalling $\psi(0) = 1$ in Eq. 3.4b, one obtains

$$u(x,t) \equiv u(x,0,t) = u_b\left(t - \frac{x}{c}\right) + u^*(x,t) \qquad (4.3)$$

Expanding the impulse response function $I(x,\tau)$ into a Taylor series around $\omega^*(x) = \omega_0$, $h^*(x) = h_0$, and then neglecting the higher-order terms for the assumption of small variation given by Eq. 3.17, and furthermore assuming independence between the material variabilities, $f(x)$, $h(x)$, and the input earthquake motion $u_b\left(t - \tau - \frac{x}{c}\right)$, one obtains the temporal spatial density spatial correlation function $P_{uu}(\xi,\omega)$ of $u(x,t)$ as follows:

$$P_{uu}(\xi,\omega) = S_{u_b u_b}(\omega) e^{-i\frac{\omega\xi}{c}} \left[\left\{\omega_0^4 + (2\beta + 4h_0^2 - 2)\omega_0^2\omega^2 + (\beta-1)^2\omega^4\right\}\left|H(\omega_0,h_0,\omega)\right|^2\right.$$

$$\left. + 4\beta^2\omega_0^4\omega^4\right\}\left\{R_{ff}(\xi) + ih_0\frac{\omega}{\omega_0}\left(r_{ff}(\xi) - R_{ff}(\xi)\right)\right.$$

$$+ h_0^2\left(\frac{\omega}{\omega_0}\right)^2\left(R_{ff}(\xi)+R_{fh}(\xi)+R_{hf}(\xi)+R_{hh}(\xi)\right)\Big]\left|H(\omega_0,h_0,\omega)\right|^4\Big] \qquad (4.4)$$

where $S_{u_b u_b}(\omega)$ is the power spectral density function of $u_b\left(t - \frac{x}{c}\right)$, and $R_{jk}(\xi)$ $(j,k = h,f)$ is the correlation function between $j(x)$ and $k(x)$ defined as $R_{jk}(\xi) = E[j(x+\xi)k(x)]$, $E[\cdot]$ = the expectation operator. The transfer function (frequency response function) $H(\omega_0,h_0,\omega)$ is given as

$$H(\omega_0,h_0,\omega) = \frac{1}{\omega_0^2 - \omega^2 + i2h_0\omega_0\omega}, \qquad i = \sqrt{-1} \qquad (4.5)$$

The temporal spectral density spatial correlation function $P_{uu}(\xi,\omega)$ in Eq. 4.4 has been derived from the following definitions:

$$P_{uu}(\xi,\omega) = \frac{1}{2\pi}\int_{-\infty}^{\infty} e^{i\omega\tau}\, Q_{uu}(\xi,\tau)d\tau \qquad (4.6a)$$

The inverse of Eq. 4.6 reclaims $Q_{u_t u_t}(\xi,\tau)$

$$Q_{uu}(\xi,\tau) = \int_{-\infty}^{\infty} e^{i\omega\tau}\, P_{uu}(\xi,\omega)d\omega \qquad (4.6b)$$

where $Q_{uu}(\xi,\tau)$ is the time-space correlation function of $u(x,t)$ defined by

$$Q_{uu}(\xi,\tau) = E[u(x+\xi,t+\tau)u(x,t)] \qquad (4.6c)$$

Parenthetically, it is noted that the spatial correlation function $R_{uu}(\xi)$ of $u(x,t)$ is defined by

$$R_{uu}(\xi) = Q_{uu}(\xi,0) = \int_{-\infty}^{\infty} P_{uu}(\xi,\omega)d\omega \qquad (4.6d)$$

which will be used later in the analysis.

In Eq. 4.4, $R_{jk}(\xi)$ and h_0 are small, and hence, again neglecting the higher orders smaller than the second-order in Eq. 4.4, Eq. 4.4 reduces to

$$P_{uu}(\xi,\omega) = S_{u_b u_b}(\omega)e^{-i\frac{\omega\xi}{c}}\left[\left\{\omega_0^4 + (2\beta+4h_0^2-2)\omega_0^2\omega^2 + (\beta-1)^2\omega^4\right\}\left|H(\omega_0,h_0,\omega)\right|^2\right.$$

$$\left. + 4\beta^2\omega_0^4\omega^4 R_{ff}(\xi)\left|H(\omega_0,h_0,\omega)\right|^4\right] \qquad (4.7)$$

Note that Eq. 4.7 will be used in a later analysis as a first-order approximation.

Integrating $P_{uu}(\xi,\omega)$, given by Eq. 4.7, with respect to ω (see Eq. 4.6d), the spatial correlation function $R_{uu}(\xi)$ of $u(x,t)$ can be obtained as

$$R_{uu}(\xi) = R_{u_1u_1}(0)\gamma_{u_1u_1}\left(\beta,h_0,\frac{\omega_0\xi}{c}\right) + R_{u_2u_2}(0)\gamma_{u_2u_2}\left(\beta,h_0,\frac{\omega_0\xi}{c}\right) \qquad (4.8)$$

where $\gamma_{u_1u_1}$ and $\gamma_{u_2u_2}$ are the spatial correlation coefficients (normalizations) of $R_{u_1u_1}(\xi)$ and $R_{u_2u_2}(\xi)$ defined by

$$R_{u_1u_1}(\xi) = \int_{-\infty}^{\infty} S_{u_1u_1}(\omega)e^{-i\frac{\omega\xi}{c}}\,d\omega \qquad (4.9a)$$

$$R_{u_2u_2}(\xi) = \int_{-\infty}^{\infty} S_{u_2u_2}(\omega)e^{-i\frac{\omega\xi}{c}}\,d\omega \qquad (4.9b)$$

and

$$S_{u_1u_1}(\omega) = \left[\omega_0^4 + (2\beta+4h_0^2-2)\omega_0^2\omega^2+(\beta-1)^2\omega^4\right]\left|H(\omega_0,h_0,\omega)\right|^2 S_{u_bu_b}(\omega) \qquad (4.9c)$$

$$S_{u_2u_2}(\omega) = 4\beta^2\omega_0^4 R_{ff}(\xi)\omega^4\left|H(\omega_0,h_0,\omega)\right|^4 S_{u_bu_b}(\omega) \qquad (4.9d)$$

If an appropriate analytical form for $S_{u_bu_b}(\omega)$ of $u_b(t)$ can be assumed, the above integrals in Eqs. 4.9a and 4.9b can be found, and eventually $R_{uu}(\xi)$ can be explicitly expressed. However, at this time, the quantitative data on

the analytical form of $S_{u_b u_b}(\omega)$ of input earthquake ground displacement $u_b(t)$ has been very limited. Hence, in the following analysis, an approximation, attractive in practice, will be devised for Eq. 4.8.

Consider the mean response displacement spectrum $S_U(\omega_a, h_a)$ of a single degree of freedom system with natural circular frequency ω_a and damping ratio h_a subjected to an input base motion displacement $u_b(t)$ (stationary random process). As is well known, (for example, Shinozuka, 1974):

$$S_U(\omega_a, h_a) = PFA_t \cdot \sqrt{\int_{-\infty}^{\infty} |H(\omega_a, h_a, \omega)|^2 S_{\ddot{u}_b \ddot{u}_b}(\omega) d\omega} \tag{4.10}$$

where $H(\omega_a, h_a, \omega)$ is the transfer function given by Eq. 5 with ω_a and h_a. The function $S_{\ddot{u}_b \ddot{u}_b}(\omega)$ is the power spectral density function of the input motion acceleration $\ddot{u}_b(t)$ and $PFA_t = PFA_t^* + 0.5772/PFA_t^*$ with

$$PFA_t^* = \sqrt{2 \ln\left(\frac{\omega_a t}{\pi}\right)} \tag{4.11}$$

in which T = duration of earthquake input motion acceleration $\ddot{u}_b(t)$. As is well known, the mean response displacement spectrum $S_u(\omega_a, h_a)$ is also related approximately to the mean response velocity spectrum $S_V(\omega_a, h_a)$ and the mean response absolute acceleration spectrum $S_A(\omega_a, _a)$ such that (for example, Clough and Penzien, 1973),

$$S_U(\omega_a, h_a) = \frac{1}{\omega_a} S_V(\omega_a, h_a), \qquad S_A(\omega_a, h_a) = \omega_a S_V(\omega_a, h_a) \tag{4.12}$$

Assuming that $S_{\ddot{u}_b \ddot{u}_b}(\omega)$ is slowly varying with ω, then the integral in Eq. 4.10 may be expressed approximately since $|H(\omega_a, h_a, \omega)|^2$ peaks at $\omega = \omega_a$ as

$$S_U(\omega_a, h_a, \omega) = PFA_t \cdot \sqrt{\frac{\pi}{2h_a\omega_a^3}}\, S_{\ddot{u}_b\ddot{u}_b}(\omega_a) \tag{4.13}$$

Similarly, $R_{u_1u_1}(0)$ and $R_{u_2u_2}(0)$ given by Eqs. 4.8 and 4.9 can be obtained approximately as

$$R_{u_1u_1}(0) = (\beta^2 + 4h_0^2)\frac{\pi}{2h_0\omega_0^3} S_{\ddot{u}_b\ddot{u}_b}(\omega_0) \tag{4.14a}$$

$$R_{u_2u_2}(0) = 4\beta^2(1 + 4h_0^2)R_{ff}(0)\frac{\pi}{16h_0^3\omega_0^3} S_{\ddot{u}_b\ddot{u}_n}(\omega_0) \tag{4.14b}$$

In the derivation of Eq. 4.14, $S_{\ddot{u}_b\ddot{u}_b}(\omega) = \omega^4 S_{u_bu_b}(\omega)$ and $S_{\dot{u}_b\dot{u}_b}(\omega) = \omega^2 S_{u_bu_b}(\omega)$ have been used. Comparing Eq. 4.13 with Eq. 4.14, Eq. 4.14 can be expressed using Eq. 4.12 as

$$R_{u_1u_1}(0) = (\beta^2 + 4h_0^2)\left[\frac{S_V(\omega_0, h_0)}{PFA_t \cdot \omega_0}\right]^2 \tag{4.15a}$$

$$R_{u_2u_2}(0) = 4\beta^2(1 + 4h_0^2)R_{ff}(0)\left[\frac{S_V(\omega_0, 8h_0^3)}{PFA_t \cdot \omega_0}\right]^2 \tag{4.15b}$$

Returning to $\gamma_{u_1u_1}(\beta, h_0, \omega_0\xi/c)$ and $\gamma_{u_2u_2}(\beta, h_0, \omega_0\xi/c)$, these functions are the correlation coefficients corresponding to the power spectral density functions $S_{u_1u_1}(\omega)$ and $S_{u_2u_2}(\omega)$ (see Eqs. 4.8 and 4.9). Recalling that the functions $S_{u_1u_1}(\omega)$ and $S_{u_2u_2}(\omega)$ in Eqs. 4.9c and 4.9d have peaks around ω_0 since $|H(\omega_0, h_0, \omega)|^2$ peaks at $\omega = \omega_0$, the apparent frequency of the processes with $S_{u_1u_1}(\omega)$ and $S_{u_2u_2}(\omega)$, defined by the square root of the normalized second moment of the power spectral density functions $S_{u_1u_1}(\omega)$ and $S_{u_2u_2}(\omega)$, may be approximately estimated as $\omega_{ap} = \omega_0$. Then, the correlation time (scale) T_0^* is given by definition as

$$T_0^* = \frac{1}{\sqrt{2}\,\pi} \cdot T_0 = \frac{1}{\sqrt{2}\,\pi} \cdot \frac{2\pi}{\omega_0} = \frac{\sqrt{2}}{\omega_0} \tag{4.16}$$

Recalling the notion of correlation time that the primary correlation struc-

ture of a stationary stochastic process can be characterized by correlation time T_0^* without knowing the detailed shape of the correlation function (Harada and Shinozuka, 1986), one may give approximations for $\gamma_{u_1u_1}$ and $\gamma_{u_2u_2}$ adopting a typical correlation function $e^{-(\tau/b)^2}$ with be = T_0^* and $\tau = \xi/c$ such that

$$\gamma_{u_1u_1} \simeq e^{-\left(\frac{ab\xi}{\sqrt{2}\,C}\right)^2} \tag{4.17a}$$

$$\gamma_{u_2u_2} \simeq \frac{R_{ff}(\xi)}{R_{ff}(0)}\, e^{-\left(\frac{\omega_0\xi}{\sqrt{2}\,C}\right)^2} \tag{4.17b}$$

Substitution of Eqs. 4.15 and 4.17 into Eq. 4.8 yields an approximate expression for $R_{uu}(\xi)$ as

$$\begin{aligned} R_{uu}(\xi) &= R_{u_1u_1}(\xi) + R_{u_2u_2}(\xi) \\ &= (\beta^2+4h_0^2)\left[\frac{S_V(\omega_0,h_0)}{PFA_t \cdot \omega_0}\right]^2 e^{-\left[\frac{\omega_0\xi}{\sqrt{2}\,C}\right]^2} \\ &\quad + 4\beta^2(1+4h_0^2)R_{ff}(\xi)\left[\frac{S_V(\omega_0,8h_0^3)}{PFA_t \cdot \omega_0}\right]^2 e^{-\left[\frac{\omega_0\xi}{\sqrt{2}\,C}\right]^2} \end{aligned} \tag{4.18}$$

Equation 4.18 shows the relationship between the spatial correlation function $R_{uu}(\xi)$ of the total ground surface displacement u(x,t), the effect of the amplitude of the ground response $S_V(\omega_0,h_0)$, the effect of the wave propagation speed c in the horizontal direction, and the spatial correlation function $R_{ff}(\xi)$ of the predominant circular ground frequency $\omega^*(x)$ resulting from the spatial variability of the soil material as well as the soil layer thickness. Equation 4.18 is quite useful for estimating the site-specific spatial variability of the ground displacement u(x,t) since the parameters on the left side of Eq. 4.18 can be easily obtained from the data available. Equation 4.7 is also useful for estimating the site-specific spatial-temporal variability of

the ground motion, provided the appropriate power spectral density function $S_{u_b u_b}(\omega)$ of the input earthquake motion $u_b(t)$ is given.

For the seismic design of buried pipelines, the maximum values of the free-field ground strains and relative displacements between two points along the horizontal (x-) axis along which the pipeline would be buried become points of major interest. Hence, the analysis that follows primarily takes advantage of such spatially related statistics as the spatial correlation function given by Eq. 4.18, without specific use of the temporal spectral density spatial correlation function given by Eq. 4.7.

5. GROUND DEFORMATION SPECTRUM

The purpose of this section is to devise the basic relationships between the ground strains and relative ground displacements which may be useful from the design point of view, on the basis of stochastic process theory.

Consider the spatial variation of free-field ground displacement along the x-axis. The total ground displacement $u(x,t)$ at a given time t is assumed to constitute a homogeneous stochastic field with zero mean and variance σ^2_{uu}. Similarly, the ground strain $\varepsilon(x,t)$ is assumed to be a homogeneous stochastic field with zero mean and variance $\sigma^2_{\varepsilon\varepsilon}$. For brevity of notation, they are denoted by $u(x)$ and $\varepsilon(x)$.

Consider first the relative displacement $u_D(x)$ between x and $x+D$:

$$u_D(x) = u(x+D) - u(x) \tag{5.1}$$

Then, the spatial correlation function $R_{u_D u_D}(\xi)$ (auto-correlation function in space) of $u_D(x)$ is given by

$$R_{u_D u_D}(\xi) = E[u_D(x+\xi)u_D(x)] \tag{5.2}$$

and can be shown to be

$$R_{u_D u_D}(\xi) = [2R_{uu}(\xi) - R_{uu}(\xi+D) - R_{uu}(\xi-D)] \tag{5.3}$$

where $R_{uu}(\xi)$ is the spatial correlation function of $u(x)$ and

$$R_{uu}(0) = \sigma^2_{uu} \tag{5.4}$$

Clearly, the variance of u_D is given by

$$\sigma^2_{u_D} = R_{u_D u_D}(0) = 2[R_{uu}(0) - R_{uu}(D)] \tag{5.5}$$

Since $R_{uu}(D) \to 0$ as $D \to \infty$,

$$\sigma^2_{u_D} = 2R_{uu}(0) = 2\sigma^2_{uu} \tag{5.6}$$

Turning to the ground strain $\varepsilon(x)$, consider the local average $\varepsilon_D(x)$ of $\varepsilon(x)$ defined by

$$\varepsilon_D(x) = \frac{1}{D}\int_x^{x+D} \varepsilon(y)dy \tag{5.7}$$

which can also be written as

$$\varepsilon_D(x) = \frac{1}{D}\, u_D(x) \tag{5.8}$$

It follows then that

$$\sigma_{\varepsilon_D} = \frac{1}{D}\,\sigma_{u_D} \tag{5.9}$$

Clearly, by definition,

$$\varepsilon_D(x) = \varepsilon(x), \qquad \sigma_{\varepsilon_D} = \sigma_{\varepsilon} \qquad \text{as } D \to 0 \tag{5.10}$$

Consideration of the asymptotic behavior of σ_{u_D} and σ_{ε_D} around $D \to 0$ and $D \to \infty$ is quite attractive to approximately describe the relationship between σ_{u_D}, σ_{ε_D} and D (Harada and Shinozuka, 1986). However, in this paper, the exact relationships given by Eqs. 5.5 and 5.9 will be considered.

While the σ_{u_D}-D relationship given by Eq. 5.5 is of definite analytical interest, the relationship between $\max(u_D)$ and D will be more useful from the design point of view, where $\max(u_D)$ indicates the maximum value of $|u_D(x)|$ over length L along the x-axis. (This notation for $\max(u_D)$ will be used for other quantities throughout this paper.) The length L is the representative linear dimension of the area in which a network of pipelines of interest exist. Hence, the mathematical question here is: What is the absolute maximum value of the free-field relative displacement $u_D(x)$ as a function of D in the one-dimensional displacement field of u(x) over the range $0 \leq x \leq L$ where

the spatial correlation function $R_{uu}(\xi)$ is known?

Similar to Eqs. 4.10 and 4.11, assuming the asymptotic largest value distribution function of the first type for $\max(u_D)$ and using its mean as the representative maximum for $\max(u_D)$, one obtains

$$\max(u_D) = PFA_s \cdot \sigma_{u_D} \tag{5.11}$$

where $PFA_s = PFA_s^* + 0.5772/PFA_s^*$ with

$$PFA_s^* = \sqrt{2\,\pi n\left(\frac{2L}{L_{u_D}}\right)} \tag{5.12}$$

where L_{u_D} is the apparent wave length L_{u_D} of $u_D(x)$ as

$$L_{u_D} = 2\pi \frac{\sigma_{u_D}}{\sigma_{u_D'}} = 2\pi \sqrt{\frac{R_{uu}(0) - R_{uu}(D)}{R_{\varepsilon\varepsilon}(0) - R_{\varepsilon\varepsilon}(D)}} \tag{5.13}$$

where $\sigma^2_{u_D'}$ is the variance of $u_D'(x)$ $(dU_D(x)/dx)$ and $R_{\varepsilon\varepsilon}(\xi)$ is the spatial correlation function of $\varepsilon(x)$. Equation 5.12 is not valid unless $L >> L_{u_D}$. (The same condition is valid for Eq. 4.11. However, in the time domain, it is usually anough that $T >> T_a = 2\pi/\omega_a$.) For small values of L, however, the mean of the peak value distribution for the $u_D(x)$ process can be used as a conservative estimate of the representative maximum. To support the assertion, consider for example the limit as $L \to 0$. In this limit, $\max(u_D)$ has the same normal distribution as $u_D(x)$ itself has. On the other hand, the peak distribution function of $u_D(x)$ is located to the right of this normal distribution. Therefore, the mean of the peak distribution function of $u_D(x)$ is larger than the mean of the distribution function for $\max(u_D)$. This is a general trend that also applies to the case in which L is fnite but small. Since the Rayleigh distribution function provides the most conservative mean amongst all the peak distribution functions having an identical standard deviation, σ_{u_D},

which is equal to $\sqrt{\pi/2}\ \sigma_{u_D}$, we assume that PFA_s is bnounded by 1.5 from below for small values of L as a conservative value of $\sqrt{\pi/2}$ (1.25). For this assumption of the bounds, PFA_s becomes a monotonically increasing function of L/L_{u_D}.

From Eq. 5.13, the apparent wave length L_{u_D} of $u_D(x)$ varies approximately between L_ε and L_u depending on the relative distance D where L_u is the apparent wave length of u(x), and L_ε is the apparent wave length of $\varepsilon(x)$ where are also similarly defined as the sqaure root of the normalized second moment of the spectral density functions of u(x) and $\varepsilon(x)$ respectively. Therefore, the PFA_s given by Eqs. 5.11 and 5.12 has the following approximate bounds:

$$\sqrt{2\ \ell n\left(\frac{2L}{L_u}\right)} + \frac{0.5772}{\sqrt{2\ \ell n\left(\frac{2L}{L_u}\right)}} \leq PFA_s \leq \sqrt{2\ \ell n\left(\frac{2L}{L_\varepsilon}\right)} + \frac{0.5772}{\sqrt{2\ \ell n\left(\frac{2L}{L_\varepsilon}\right)}} \tag{5.14}$$

From the design point of view, the upper bound $PFA^*_{su} + 0.5772/PFA^*_{su}$ with

$$PFA^*_{su} = \sqrt{2\ \ell n\left(\delta \cdot \frac{2L}{L_u}\right)} \tag{5.15}$$

is of more interest, where $\delta = L_u/L_\varepsilon$. However, in order to derive the upper bound, one must estimate L_ε. This requires knowledge of the auto-correlation function of the strain itself which in turn requires the derivative of u(x). Obviously, such information will not be available in practice. Alternatively, L_ε can be obtained in terms of the second and fourth spectral moments of u(x). The spectral density function, however, can only be constructed through the Wiener-Khintchine transform of the auto-correlation function $R_{uu}(\xi)$ of u(x). Since at best $R_{uu}(\xi)$ can be estimated only in approximation and since the spectral moments can be highly sensitive to the analytical forms of the spectral density function $S_{uu}(\kappa)$, the alternative method of estimating L_ε also suffers from some uncertainty in the absence of a robust data base. Hence, it

is recommended here that the following value be used for δ.

$$\delta = 2.5 \tag{5.16}$$

The value of δ in Eq. 5.16 was chosen from the following results, associated with the particular forms of the spatial correlation function listed below:

$$\delta = \frac{L_u}{L_\varepsilon} = \sqrt{6} = 2.5 \qquad \text{for } R_{uu}(\xi) = \frac{b^2}{\xi^2+b^2} \tag{5.17a}$$

$$= \sqrt{5/2} = 1.6 \qquad \text{for} \qquad = \frac{b^4(b^2-3\xi^2)}{(\xi^2+b^2)^3} \tag{5.17b}$$

$$= \sqrt{3} = 1.7 \qquad \text{for} \qquad = e^{-\left(\frac{\xi}{b}\right)^2} \tag{5.17c}$$

$$= \sqrt{5/3} = 1.3 \qquad \text{for} \qquad = \left[1-2\left(\frac{\xi}{b}\right)^2\right]e^{-\left(\frac{\xi}{b}\right)^2} \tag{5.17d}$$

Note that Eq. 5.15 gives, in approximation, the lower bound of PFA^*_{su} when δ = 1. From Harada and Shinozuka, 1986, Eq. 5.15 with δ = 2.5 gives a good approximation for the peak factor PFA^*_s given by Eq. 5.12.

In Fig. 1, the variation of PFA^*_{su} given by Eq. 5.15 with δ = 2.5 with respect to the parameters is shown together with that of PFA^*_t given by Eq. 4.11. It is found from Fig. 1 that the variation of PFA^*_{su} and PFA^*_t is slow. Hence, from the practial application point of view, it may be assumed that $PFA^*_{su} = PFA^*_t$ is eventually $PFA_s = PFA_t$.

Summarizing Eqs. 5.5, 5.9, 5.11 and 5.15, one obtains

$$\max(u_D) = PFA_s \cdot \sigma_{u_D} = \sqrt{2} \cdot PFA_s \cdot \sqrt{R_{uu}(0) - R_{uu}(D)} \tag{5.18}$$

$$\max(\varepsilon_D) = \frac{1}{D}\max(u_D) \tag{5.19}$$

Plotting $\max(u_D)$ as a function of D in log-log scale, $\max(\varepsilon_D)$ can be read from the axis going down from the right to left since Eq. 5.19 exists. Hereafter, the $\max(u_D)$0-$\max(\varepsilon_D)$-D diagram plotted in log-log scale is called the ground deformation spectrum. Several examples of the ground deformation spectrum

constructed from the statistical analysis of seismic array data and permanent ground deformation data due to earthquakes can be seen in the papers by Harada et al., 1984, Harada and Shinozuka, 1986. In the following analysis, combining Eqs. 4.18 with Eqs. 5.18 and 5.19, we will construct a site-specific ground deformation spectrum for illustrating a practical application of Eq. 4.18.

6. NUMERICAL EXAMPLE

In order the explain the utilization of Eq. 4.18 when estimating a site-specific ground deformation spectrum, consider a site where the soil conditions are as shown in Fig. 1 and Table 1. Therein, the model ground (1200 x 70 m x m) consists of six different layers with materials shown in Table 1. The bottom of the ground surface is assumed to be rigid. The ground is divided in the horizontal direction into sixty sections where each section has 20 m (20 = 1200/60) as shown in Fig. 1. From the layer thickness and soil material data shown in Fig. 1 and Table 1 in each soil section, the predominant ground frequency $\omega^*(x_n)$ (n = 1,2,...,60) can be computed using Eq. 3.20 in each soil section (x_n = location of soil section from left side of Fig. 1). The mean value ω_0 and coefficient of variation of $\omega^*(x_n)$ are estimated as

$$\tilde{\omega}_0 = 2\pi f_0 = 2\pi \times 0.89 = 5.59 \text{ (rad/s)} = (T_0 = 1.12 \text{ sec}) \tag{6.1}$$

$$\tilde{\delta}_{\omega^*} = 0.085 \tag{6.2}$$

The sample spatial correlation function $\tilde{R}_{ff}(\xi_k)$ of f(x) is calculated by interpreting the sample $\omega^*(x_n)$ as a realization of the homogeneous stochastic process $\omega^*(x)$ using the following equation:

$$\tilde{R}_{ff}(\xi_k) = \frac{1}{N-k} \sum_{n=1}^{N-k} [\omega^*(x_n+\xi_k) - \omega_0][\omega^*(x_n) - \omega_0] \tag{6.3}$$

where N = total number of soil sections (60). To avoid a small averaging number N-k in Eq. 3, ξ_k = 600 (m) is used as the longest separation distance, and therefore, k = 0, 1, 2, ..., 30 (30 = 600/20) where $\xi_0 = 0$, $\xi_1 = 20$, $\xi_2 = 40$, ..., $\xi_{30} = 600$. The resulting normalized spatial correlation function $\tilde{R}_{ff}(\xi_k)/\tilde{R}_{ff}(0)$, ($\tilde{R}_{ff}(0) = \tilde{\sigma}^2_{ff} = \tilde{\delta}^2_{\omega^*} = 0.085 \times 0.085$, see Eq. 3.18) is plotted by the solid curve in Fig. 2.

Parenthetically, it is noted that the ground response displacements are calculated for the same ground model with element sizes as shown in Fig. 1 using the finite element method (Harada and Sakamoto, 1985). In calculating the response displacements, constant soil material damping is assumed in each soil layer as 5% of the critical damping. To represent the infinite horizontal ground, the transmitting boundary is equipped on both sides (left and right) of the model ground shown in Fig. 1. At the rigid bottom of the ground model, the earthquake acceleration time history as shown in Fig. 3 is inputted with peak acceleration 10 (cm/s^2). The sample spatial correlation function $\tilde{R}_{u_2u_2}(\xi_k)$ of the ground surface displacement $u_2(x,t)$ (= $u(x,t) - \bar{u}(t)$ where $u(x,t)$ = total ground surface displacement and $\bar{u}(t)$ = spatial average displacement of $u(x,t)$) is estimated by:

$$\tilde{R}_{u_2u_2}(\xi_k) = \frac{1}{T(N-k)} \sum_{n=1}^{N-k} \int_0^T [u(x_n+\xi_k,t) - \bar{u}(t)][u(x_n,t) - \bar{u}(t)]dt \qquad (6.4)$$

where $\bar{u}(t)$ is estimated as

$$\bar{u}(t) = \frac{1}{N} \sum_{n=1}^{N} u(x_n,t) \qquad (6.5)$$

The resulting normalization $\tilde{R}_{u_2u_2}(\xi_k)/\tilde{R}_{u_2u_2}(0)$ is also plotted in Fig. 2 by a dashed curve.

In the above response analysis, the wave propagation speed is assumed as $c = \infty$ (the same input motion is subjected to ground surface motion from the rigid base rock). Hence, from Eq. 4.18, the spatial correlation function $R_{u_2u_2}(\xi)$ of $u_2(x,t)$ is

$$R_{u_2u_2}(\xi) = 4\beta^2(1+4h_0^2)R_{ff}(\xi)\left[\frac{S_V(\omega_0,8h_0^3}{PFA_t \cdot \omega_0}\right]^2 \qquad (6.6)$$

Therefore, the normalized spatial correlation function $R_{u_2u_2}(\xi)/R_{u_2u_2}(0)$ becomes identical with the normalized spatial correlation function $R_{ff}(\xi)/R_{ff}(0)$. The relatively good agreement between $\tilde{R}_{u_2u_2}(\xi_k)/\tilde{R}_{u_2u_2}(0)$ calculated by FEM and $\tilde{R}_{ff}(\xi_k)/\tilde{R}_{ff}(0)$ estimated from $\omega^*(x_n)$ indicates that the response spactral correlation function $R_{u_2u_2}(\xi)$ is proportional to the spatial correlation function $R_{ff}(\xi)$ of the predominant ground frequency $\omega^*(x)$ as expected from Eq. 6.6.

To approximately represent the behavior of the spatial correlation function $R_{ff}(\xi)$ shown in Fig. 2 (solid curve), an (appropriate) analytical form is assumed such that

$$R_{ff}(\xi) = \sigma_{ff}^2\left[1 - 2\left(\frac{\xi}{b}\right)^2\right]e^{-\left(\frac{\xi}{b}\right)^2} \qquad (6.7)$$

with $\sigma_{ff} = \delta_{\omega^*} = 0.085$, $b = 141.42$ (m). The value of b is determined in such a way that Eq. 6.7 is zero at $\xi = 100$ m. Substituting Eq. 6.7 into Eq. 4.18, the spatial correlation function $R_{uu}(\xi)$ of the ground surface displacement $u(x,t)$ for a site with soil layers as shown in Fig. 1 can be estimated as

$$R_{uu}(\xi) = \left(\beta^2+4h_0^2\right)\left[\frac{S_V(\omega_0,h_0)}{PFA_t \cdot \omega_0}\right]^2 e^{-\left[\frac{\omega_0\xi}{\sqrt{2}\,c}\right]^2}$$

$$= 4\beta^2(1+4h_0^2)\left[\frac{S_V(\omega_0,8h_0^3}{PFA_t \cdot \omega_0}\right]^2\sigma_{ff}^2\left[1-2\left(\frac{\xi}{b}\right)^2\right]e^{-\left(\frac{\xi}{b}\right)^2} e^{-\left(\frac{\omega_0\xi}{\sqrt{2}\,c}\right)^2} \qquad (6.8)$$

Now, assuming the following parameters in addition to the values given by Eqs. 6.1, 6.2 and 6.7, the response velocity spectrum per unit input acceleration = Fig. 4 (this spectrum was proposed by the Public Works Research Institute, Ministry of Construction, 1970 as the averages from numerous ground motion records measured in stiff ground), the mean damping rate h_0 for the

ground = 0.18, participation factor $\beta = 4/\pi$, input peak acceleration at base rock = 200 (cm/s^2), wave propagation speed c = 1500 (m/s), duration of input motion T = 10 (sec), one can then calculate the parameters in Eq. 6.8 and, substituting these parameter values into Eq. 6.8, one obtains

$$R_{uu}(\xi) = R_{u_1u_1}(\xi) + R_{u_2u_2}(\xi)$$
$$= 2.1e^{-(\frac{\xi}{279.3})^2} + 0.26[1 - 2(\frac{\xi}{141.42})^2]e^{-(\frac{\xi}{132.3})^2} \quad (6.9)$$

The spatial correlation function $R_{\varepsilon\varepsilon}(\xi)$ of the ground strain $\varepsilon(x) = \partial u(x)\partial x$ can be obtained from $R_{uu}(\xi)$ as

$$R_{\varepsilon\varepsilon}(\xi) = \frac{d^2R_{uu}(\xi)}{d\xi^2} = R_{\varepsilon_1\varepsilon_1}(\xi) + R_{\varepsilon_2\varepsilon_2}(\xi)$$
$$= 0.29 \times 10^{-8}[1 - 2(\frac{\xi}{379.3})^2]e^{-(\frac{\xi}{379.3})^2} + 3.14 \times 10^{-8} \times$$
$$\times [1 - (\frac{\xi}{67.0})^2 + (\frac{\xi}{124.7})^4]e^{-(\frac{\xi}{132.5})^2} \quad (6.10)$$

From Eqs. 5.18 and 6.10, one obtains

$$\max(u_D) = 2.64 \times \sqrt{2} \cdot \sqrt{2.36 - 2.1e^{-(\frac{\xi}{379.2})^2} - 0.26[1 - 2(\frac{\xi}{141.42})^{-2}]e^{-(\frac{\xi}{132.5})^2}} \quad (6.11)$$

In Eq. 6.11, $PFA_s = PFA_t = 2.64$ is assumed.

In Fig. 5, the values of Eqs. 6.9 and 6.10 are plotted for $R_{uu}(\xi)$, $R_{u_1u_1}(\xi)$, $R_{u_2u_2}(\xi)$, $R_{\varepsilon\varepsilon}(\xi)$, $R_{\varepsilon_1\varepsilon_1}(\xi)$ and $R_{\varepsilon_2\varepsilon_2}(\xi)$. It is observed from Fig. 1 that the strain correlation function $R_{\varepsilon\varepsilon}(\xi)$ is primarily governed by the $R_{\varepsilon_2\varepsilon_2}(\xi)$ associated with the ground displacement $u_2(x,t)$ due to the spatial variability of the predominant ground frequency, while the displacement correlation function $R_{uu}(\xi)$ is entirely controlled by $R_{u_1u_1}(\xi)$ of the ground displacement $u_1(x,t)$ due to wave propagation.

In Fig. 6, the ground deformation spectra given by Eq. 11 are plotted corresponding to $R_{uu}(\xi)$, $R_{u_1u_1}(\xi)$ and $R_{u_2u_2}(\xi)$. It is again observed from Fig. 6 that the maximum ground strain $\max(\varepsilon_D)$ is mainly controlled by the ground displacement $u_2(x,t)$ originating in the spatial variability of the predominant ground frequency, while the maximum relative displacement $\max(u_D)$ by $u_1(x,t)$ is due to wave propagation.

7. CORRELATION BETWEEN AXIAL GROUND STRAIN AND DAMAGE STATISTICS

The purpose of this section is to demonstrate the capability of the analytical spatial correlation function $R_{uu}(\xi)$ given by Eq. 4.18 by showing a correlation between the rms (root mean square) axial ground strain $\sigma_{\varepsilon\varepsilon}$ evaluated from Eq. 4.18 and the damage statistics of buried water supply pipelines under the 1923 Kanto earthquake. Since the ground strain is almost controlled by $R_{u_2u_2}(\xi)$ in Eq. 4.18 as suggested in the numerical example section (6), for simplicity, the ground strain in this study is estimated from $R_{u_2u_2}(\xi)$ in Eq. 4.18, neglecting the effect of wave propagation ($c = \infty$). Hence the ground strain considered hereafter is associated with the effect of the ground amplification S_V and the effect of the spatial variability of the predominant ground frequency $\omega^*(x)$ characterized by the spatial correlation function $R_{ff}(\xi)$ of $\omega^*(x)$. A similar study has already been done (Shinozuka and Kawakami, 1977) using a numerically simulated rms ground strain calculated from a one-dimensional propagating shear wave model, but the study presented in this section is based on the theoretical equation given by Eq. 4.18.

In damage statistics studies (Kubo and Katayama, 1975), the predominant ground frequencies are evaluated at the nodal points of a grid of meridians and parallels (both at intervals of 1 km) covering the Tokyo metropolitan area. The evaluation is made based on soil conditions at the nodes under the shear beam assumption, and for each area element of 1 km^2, the average $\bar{f}_0$ and the standard deviation $\tilde{\sigma}_{f^*f^*}$ of the predominant frequency are computed using frequencies evaluated at its four corners.

The study then examines the statistics taken from an underground water supply pipeline system which was in service at the time of the 1923 Kanto earthquake and counts the number of pipe breaks and leaks in each area element resulting from the same earthquake. These numbers are divided by the length

(in km) of the pipelines in each area to obtain the "break damage index" DI or the "leakage damage index." Furthermore, the study correlates $\tilde{f}_0$ and $\tilde{\sigma}_{f^*f^*}$ to DI by dividing the $\tilde{f}_0$ and $\tilde{\sigma}_{f^*f^*}$ space into the following four regions as shown in Table 1. The quantity $\overline{DI}$ in Table 1 indicates the average value of DI in each region. Table 1 shows that region III produces the most damage statistics while region I is the second worst. The damage indices associated with regions II and IV are much smaller than those with region III.

This Japanese data implicitly assuems that the variation of the predominant frequency is two-dimensional, i.e., $f^* = f^*(x,y)$. Although it may not be extremely difficult to deal with such a two-dimensional model, the aount of assumptions required to construct it would be inconsistent with the quality and quantity of the available field data. Therefore, as seen in the study by Shinozuka and Kawakami (1977), the rpesent study also deals with the case where the predominant frequency f^* varies only in the x-direction, i.e., $f^* = f^*(x)$ and where f^* is evaluated along the x-axis at equal intervals of 1 km. This procedure is a one-dimensional equivalent of the Japanese study such that the predominant frequency in each interval of 1 km varies as the stochastic field $f^*(x)$. Under these circumstances, it is considered as a first approximation that the mean f_0 and the standard deviation $\sigma_{f^*f^*} = f_0\delta_{\omega^*}$ (δ_{ω^*} = the coefficient of variation of $\omega^*(x) = 2\pi f^*(x)$ to be used for an interval are equal respectively to the sample mean $\tilde{f}_0$ and the sample standard deviation $\tilde{\sigma}_{f^*f^*}$ obtained on the basis of the predominant frequencies evaluated at both ends of that interval.

Similar to the procedure illustrated inthe numerical example in Section 6, assuming $b = \sqrt{3} \times 100$, (173.2 m), $c = \infty$, $T = 10$ (sec), $h_0 = 0.3$, input peak acceleration = 200 (cm/s^2), and the response velocity spectrum for unit input acceleration as shown in Fig. 6.4 in Eq. 6.8, the rms (root mean square)

ground strain $\sigma_{\varepsilon\varepsilon}$ is computed for various combinations of the mean $f_0(\omega_0/2\pi)$ and standard deviation $\sigma_{ff^*} = f_0\delta_{\omega^*}$ of the predominant ground frequency; f_0 = 0.75, 1.25, 1.75, ..., 6.75 (Hz) and $\sigma_{f^*f^*} = f_0\delta_{\omega^*}$ = 0.125, 0.375, 0.625, ..., 3.125 (Hz). Purely for the purpose of establishing a trend, it is assumed that a particular combination of $\tilde{f}_0$ and $\tilde{\sigma}_{f^*f^*}$ under the assumption of two-dimensional variation of f*(x,y) will produce the same rms ground surface strain as those computed from Eq. 6.8. The computed results are then used in conjunction with the Japanese data, particularlyu with those given in FIg. 1 which shows the number of area elements of 1 km square associated with the indicated combinations of $\tilde{f}_0$ and $\tilde{\sigma}_{f^*f^*}$ with blanks implying zero; $\tilde{f}_0$ = 0.75, 1.25, 1.75, ..., 6.75 (Hz) and $\tilde{\sigma}_{f^*f^*}$ = 0.125, 0.375, 0.625, ..., 3.125 (Hz) (these values are the same as those for f_0 and $\sigma_{f^*f^*} = f_0\delta_{\omega^*}$). Thus, the $\tilde{f}_0$-$\tilde{\sigma}_{f^*f^*}$ planes divided as shown in Fig. 1 correspond to the four regions, I, II, III, and Iv as empirically defined in Table 1.

The weighted averages of the rms ground strains within regions I-IV are then calculated with the numbers shown in Fig. 1 as weight. These averages will be referred to as the "regional rms ground strain." They are shown in Table 2 and Fig. 2 together with those for b = $\sqrt{3}$ x 150 (260), $\sqrt{3}$ x 250 (433), and $\sqrt{3}$ x 350 (606), (m). Figure 2 shows that the regional rms ground strains are larger for small values of b within individual regions as expected, and that relatively larger values are observed in regions I and III, the smaller values in regions II and IV exhibiting a trend relatively similar to that observed in the Japanese damage statistics in Table 1.

A similar trend is also found in the numerical simulation studies by Shinozuka and Kawakami (1977) shown in Fig. 3 where the parameter L corresponds to b. The trend is even more similar to the damage statistics if we take into account the following: assuming a smaller value of b for region III

then for the other regions may be more realistic since the soil conditions of region III generally consist of more irregular soil layers including buried valleys and tablelands and are expected to be more irregular than in those in other regions. For example, take the rms values associated with $b = \sqrt{3} \cdot 100$ (173 m) for region III while the rms values with $b = \sqrt{3} \cdot 350$ (606 m) for other regions, and observe how closely the results (see Fig. 4) compare with the damage statistics trend indicated in Fig. 2b.

9. CONCLUSIONS

Aiming at a characterization of the spatial variability of ground motions for the seismic analysis and design of long extended buried lifeline structures such as gas, electric and water supply pipelines, this paper has developed a simple stochastic ground resopnse model for earthquake excitations where the soil thickness and soil material are random functions of the horizontal coordinate. From this model, we can estimate the ground response spatial variabilities, provided that there is a response velocity spectrum, a spatial correlation function of the predominant ground frequency varying with the horizontal location, wave propagation speed in horizontal direction, mean value of equivalent damping of ground and mean value of the predominant ground frequency. The analytical solution is based on the widely used perturbation method and its accuracy checked with the finite element solution method. Also, the root mean square (rms) values of the ground strain from the analytical solution developed in this study are compared with the statistics of earthquake-induced damage based on a field study of underground water supply pipelines in Tokyo. The comparison indicates that good correlation exists between the rms values of the ground strain and the degree of damage.

ACKNOWLEDGEMENT

This work was supported by the Tokyo Gas Company, Ltd., Tokyo, Japan.

The views, opinions and findings expressed in this study are those of the authors and should not be construed as representing an official position, policy or decision on the part of the organization mentioned above.

REFERENCES

1. Bard, P. and Bouchon, M., "The Seismic Response of Sediment-Filled Valleys," Bulletin of the Seismological Society of America, Vol. 70, No. 5, 1980, pp. 1921-1941.

2. Earthquake Engineering Committee (JSCE), "Earthquake-Resistant Design for Civil Engineering Structures in Japan; Earthquake-Resistant Design Features of Submerged Tunnels in Japan," JSCE, 1984.

3. Harada, T., "Probabilistic Modelig of Spatial Variation of Strong Earthquake Ground Displacements," Proceedings of the 8th World Conference on Earthquake Engineering, 1984, pp. 605-612.

4. Harada, T. and Shinozuka, M., "Ground Deformation Spectra," Proceedings of the 3rd U.S. National Conference on Earthquake Engineering, 1985.

5. Harada, T. et al., "Preliminary Study on Spatial Variation of Ground Deformation for Seismic Design of Buried Lifeline Structures," Public Works Research Institute, Report No. 2143, Ministry of Construction, Japan, 1984 (in Japanese).

6. Japan Road Association, "Earthquake-Resistant Design Specifications of Highway Bridges," 1980.

7. Kanai, K., Engineering Seismology, (Tokyo: University of Tokyo Press), 1983.

8. Kausel, E. and Pais, A., "Deconvolution of Stochastic SH-Wave Motions in Soil Deposits," Research Report R84--09, Dept. of Civil Engineering, MIT, 1984.

9. Kubo, K. and Katayama, T., "Survey on Underground Pipe Damages Due to Earthquake," Tokyo Metropolitan Disaster Prevention Congress, Governor's Office, The Metropolitan Government of Tokyo, 1975 (in Japanese).

10. Kubo, K., Katayama, . and Ohashi, M., "Lifeline Earthquake Engineering in Japan," Journal of the Technical Councils, ASCE, Vol. 105, No. TC1, 1979, pp. 221-238.

11. Loh, C.H., Penzien, J. and Tsai, Y.B., "Engineering Analyses of SMART-1 Array Accelerograms," Earthquake Engineering and Structural Dynamics, Vol. 10, 1982, pp. 575-591.

12. Okamoto, S., Introduction to Earthquake Engineering, (Tokyo: University of Tokyo Press), Tokyo, 1984, second edition.

13. Shinozuka, M. and Kawakami, H., "Ground Characteristics and Free-Field Strains," Technical Report No. CU-2, Dept. of Civil Engineering and Engineering Mechanics, Columbia University, 1977.

14. Shinozuka, M., "Safety Against Dynamic Forces," Journal of the Structural Division, ASCE, Vol. 100, No. ST9, 1974, pp. 1821-1826.

Table 6-1 Material Properties Used in Numerical Example

Layer (1)	Soil Mass g/cm^2 (2)	Poisson Ratio (3)	Shear Modulus kg/cm^2 (4)	Shear Wave Velocity m/s (5)
1 Sand	1.80	0.48	133.0	85
2 Sand	1.70	0.48	287.0	125
3 Clay	1.50	0.48	612.0	200
4 Gravel	1.90	0.48	2050.0	325
5 Sand-stone	2.10	0.48	5360.0	500
6 Sand-stone	2.20	0.48	14367.0	800

Table 7-1 Break Damage Index for Four Regions

Regions (1)	$\hat{f}_0$ (Hz) (2)	$\hat{\sigma}_{f^*f^*}$ (Hz) (3)	$\overline{DI}$ (4)
I	1.5 - 3.5	0 <	5.1
II	3.5 - 4.5	0 - 1.15	2.6
III	3.5 - 4.5	1.15 <	13.3
IV	4.5 - 5.5	0 <	2.8

Table 7-2 Regional rms Ground Strains ($x10^{-4}$)

	Parameter b (m)				
Regions (1)	$100\sqrt{3}$ (2)	$150\sqrt{3}$ (3)	$250\sqrt{3}$ (4)	$300\sqrt{3}$ (5)	$350\sqrt{3}$ (6)
I	2.39	1.59	0.96	0.80	0.68
II	1.05	0.70	0.42	0.35	0.30
III	1.85	1.23	0.74	0.62	0.53
IV	0.82	0.55	0.33	0.27	0.23

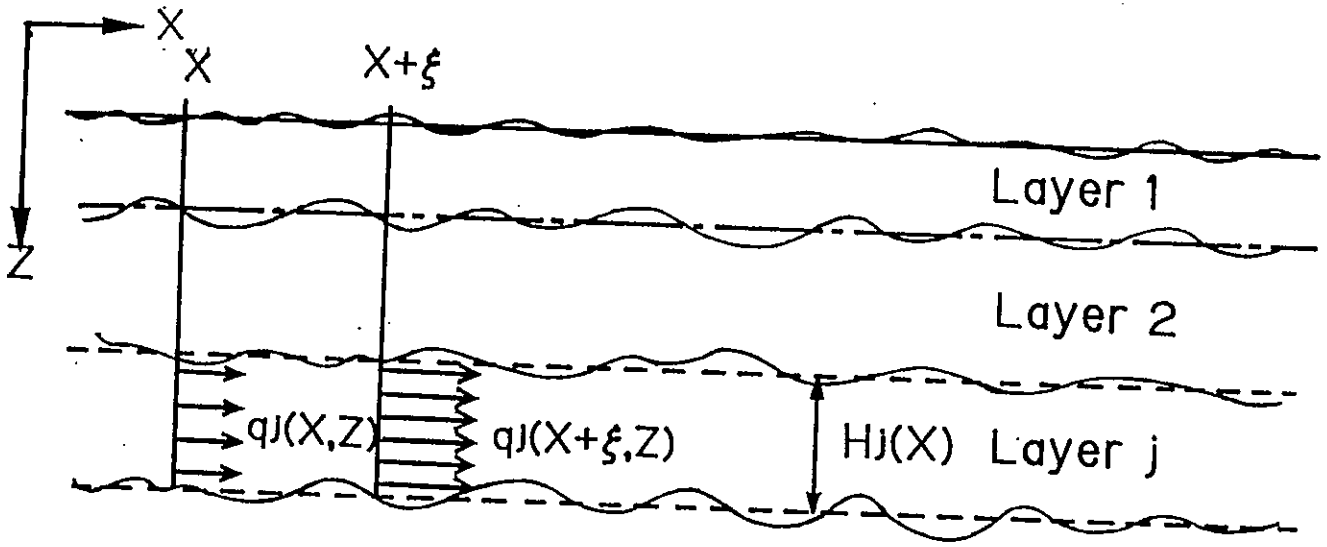

Fig. 2-1 Horizontal Soil Layers Showing Layer Depth $H_j(x)$ and Soil Property $q_j(x,z)$

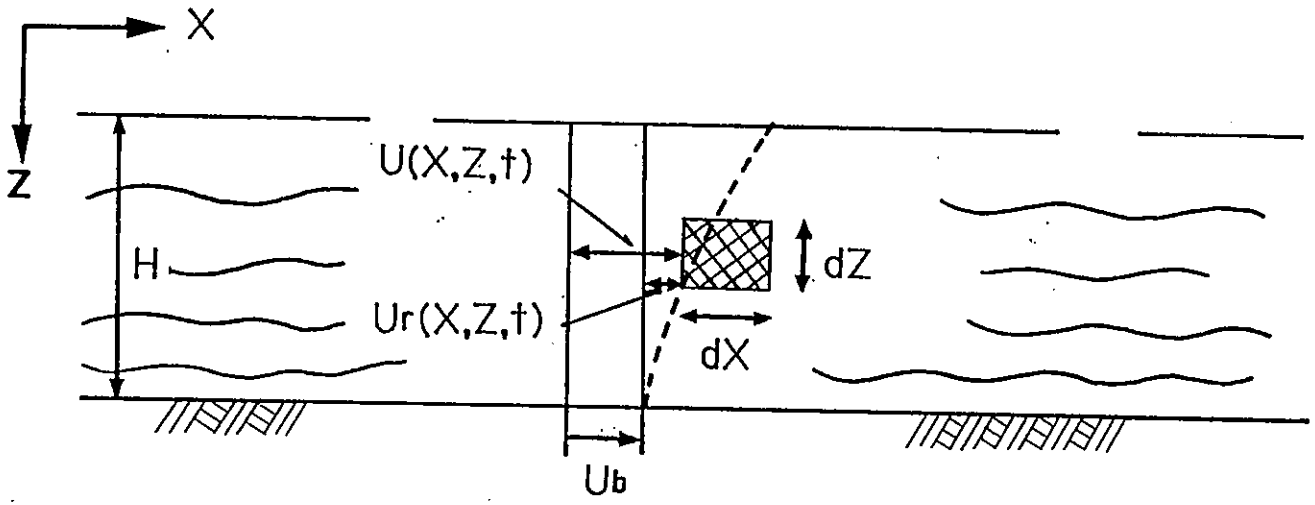

Fig. 3-1 Mathematical Model of The Horizontally Homogeneous Ground And Its Notation.

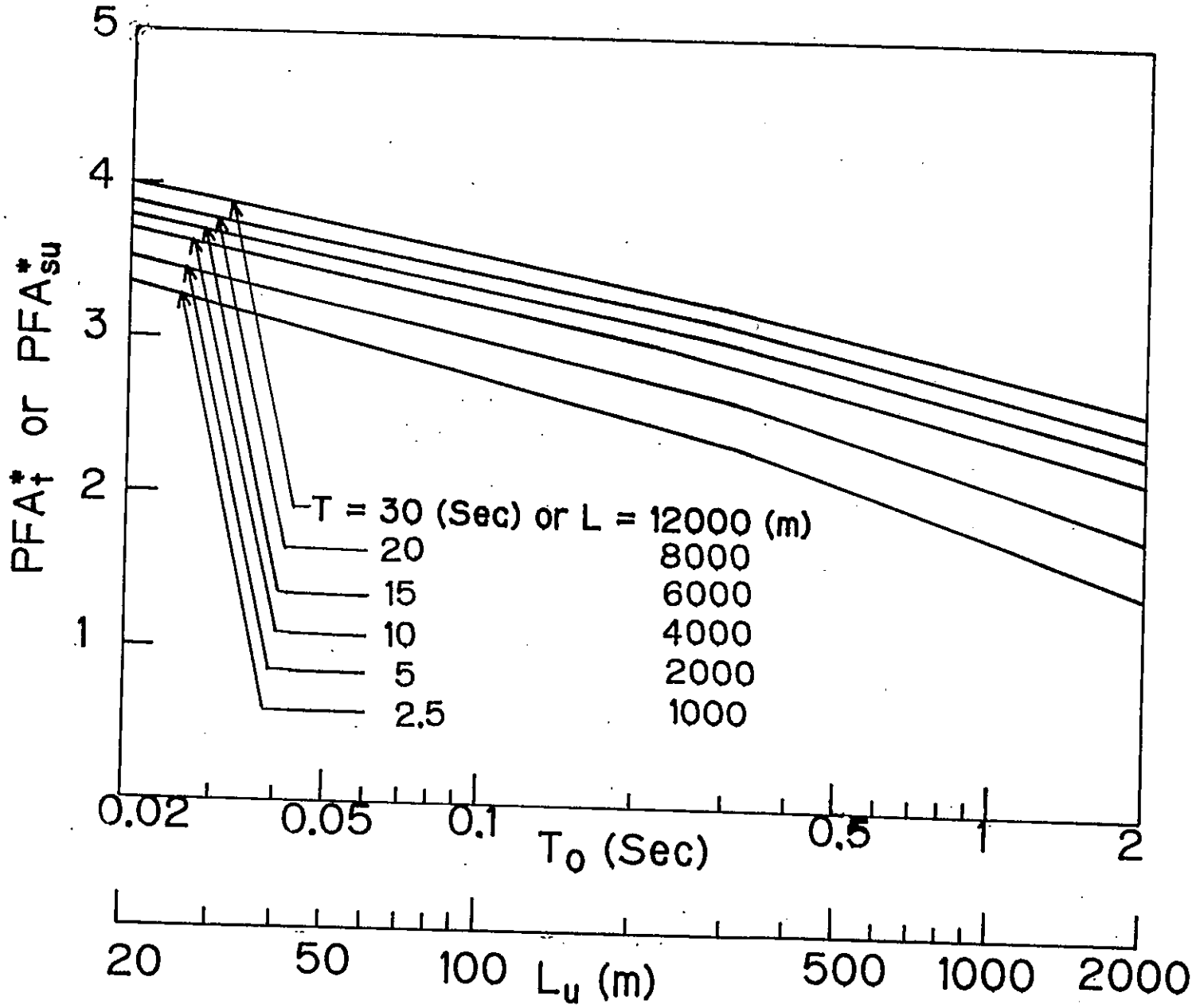

Fig. 5-1 Variation of Peak Factors With Parameters

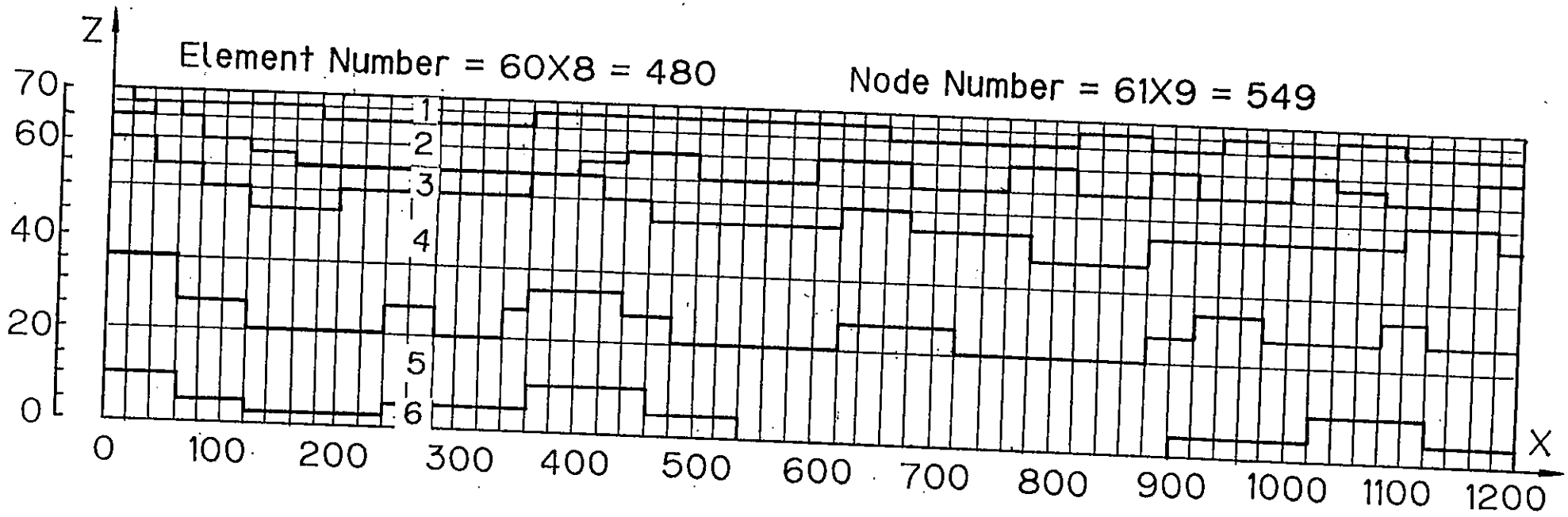

Fig. 6-1 Ground Model Used in Numerical Example

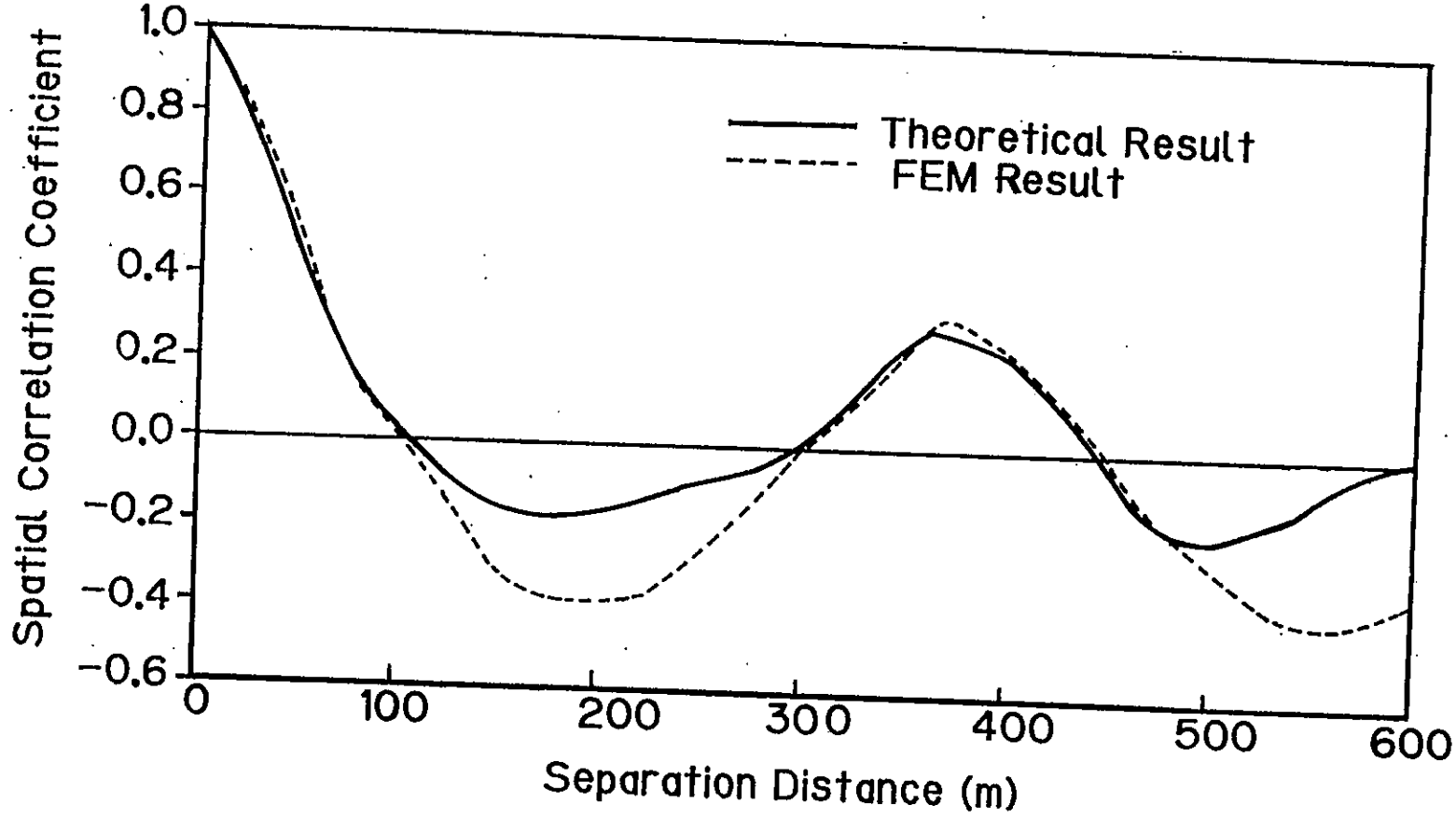

Fig. 6-2 Comparison of The Theoretical and Numerical Spatial Correlation Coefficients

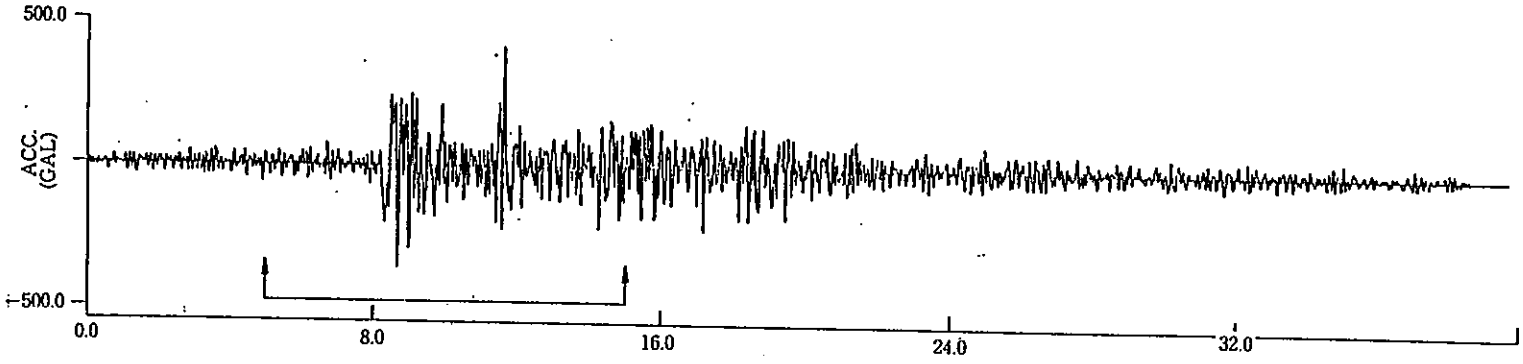

Fig. 6-3 Input Acc. Time History (Portion of 10 sec. indicated by ▲——▲ is used)

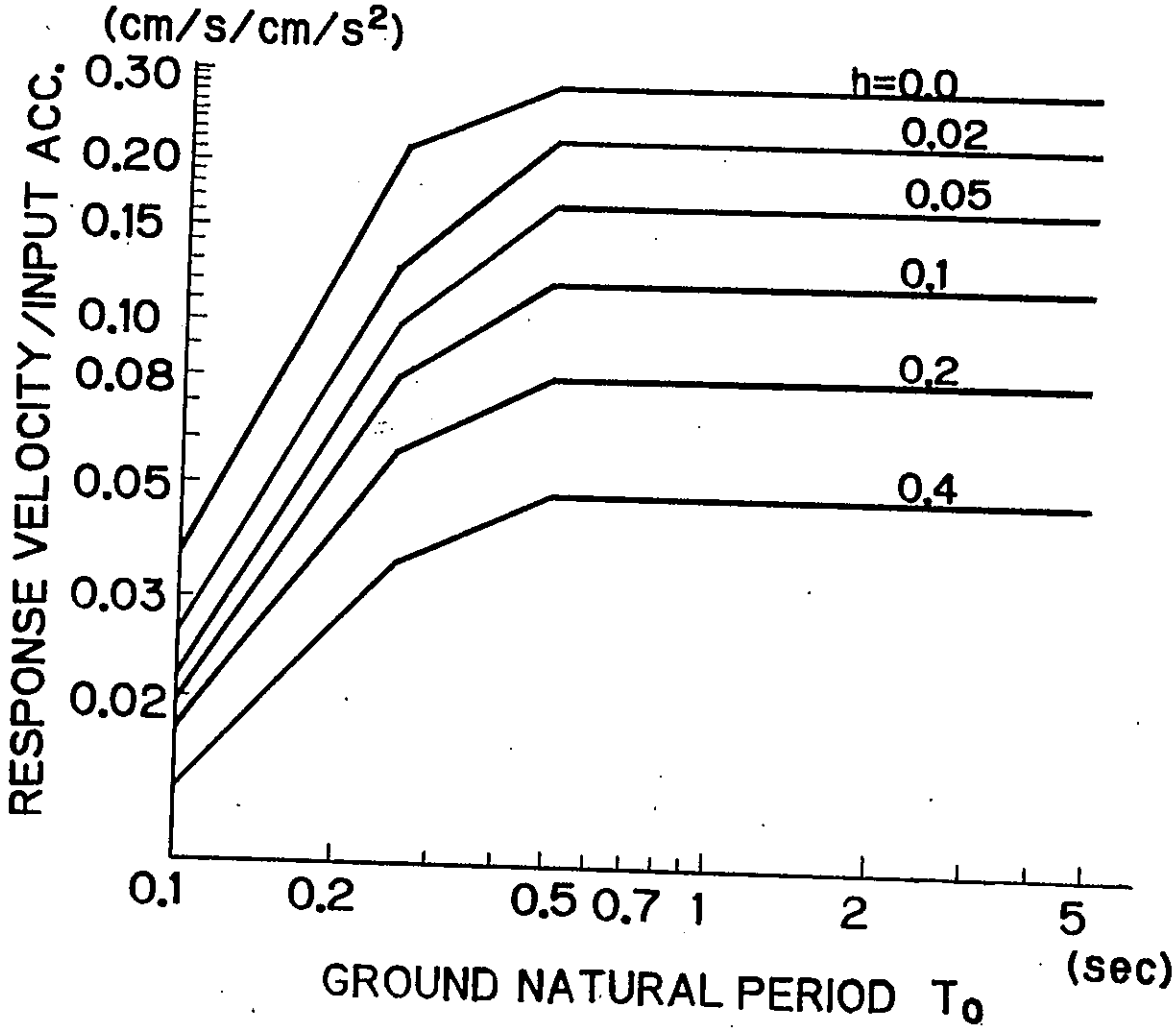

Fig.6-4 Response Velocity Spectra for Unit Input Acceleration Proposed by Public Works Research Institute, Ministory of Construction

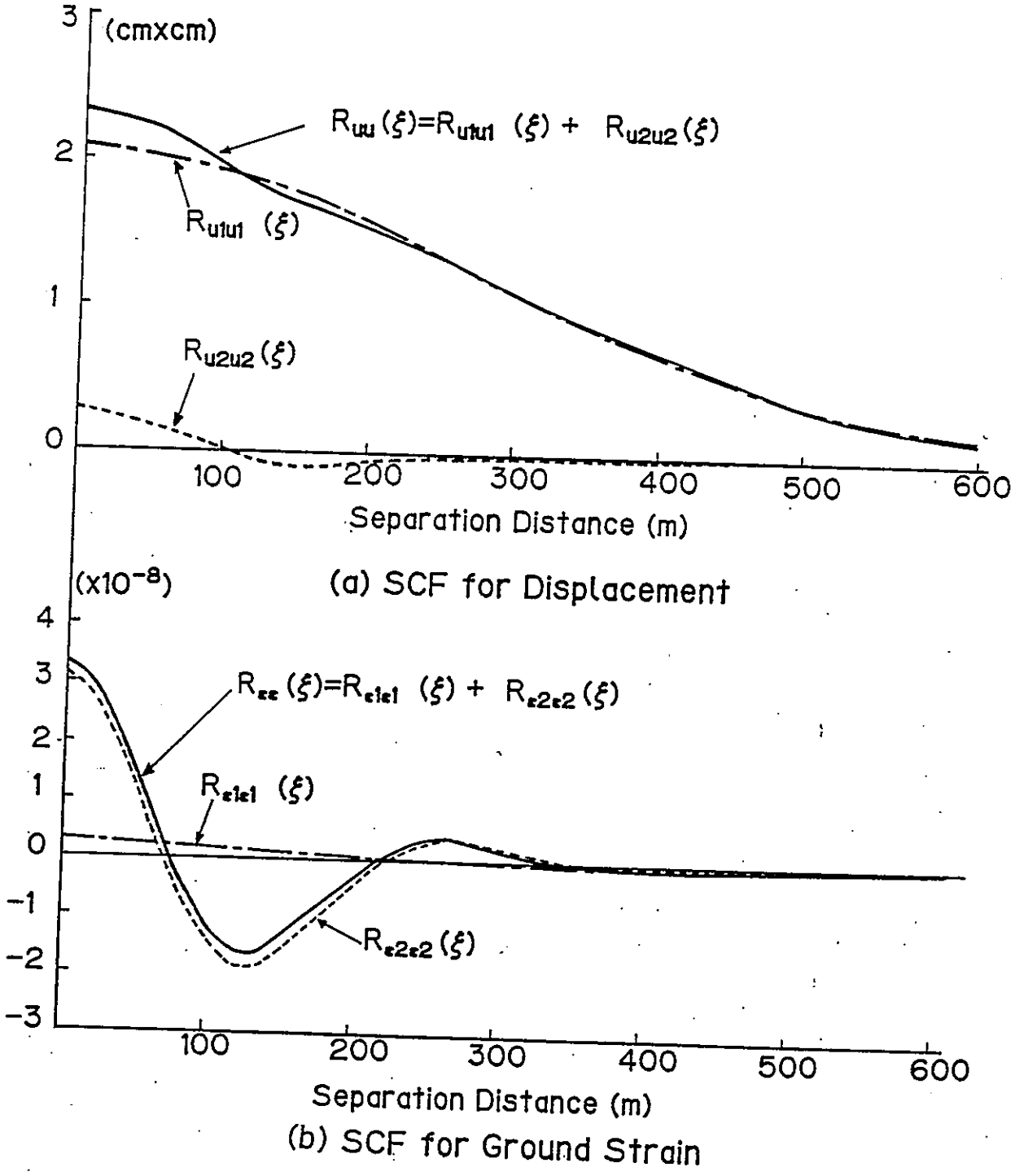

Fig. 6-5 Examples of Spatial Correlation Functions for Ground Surface Displacement and Ground Strain

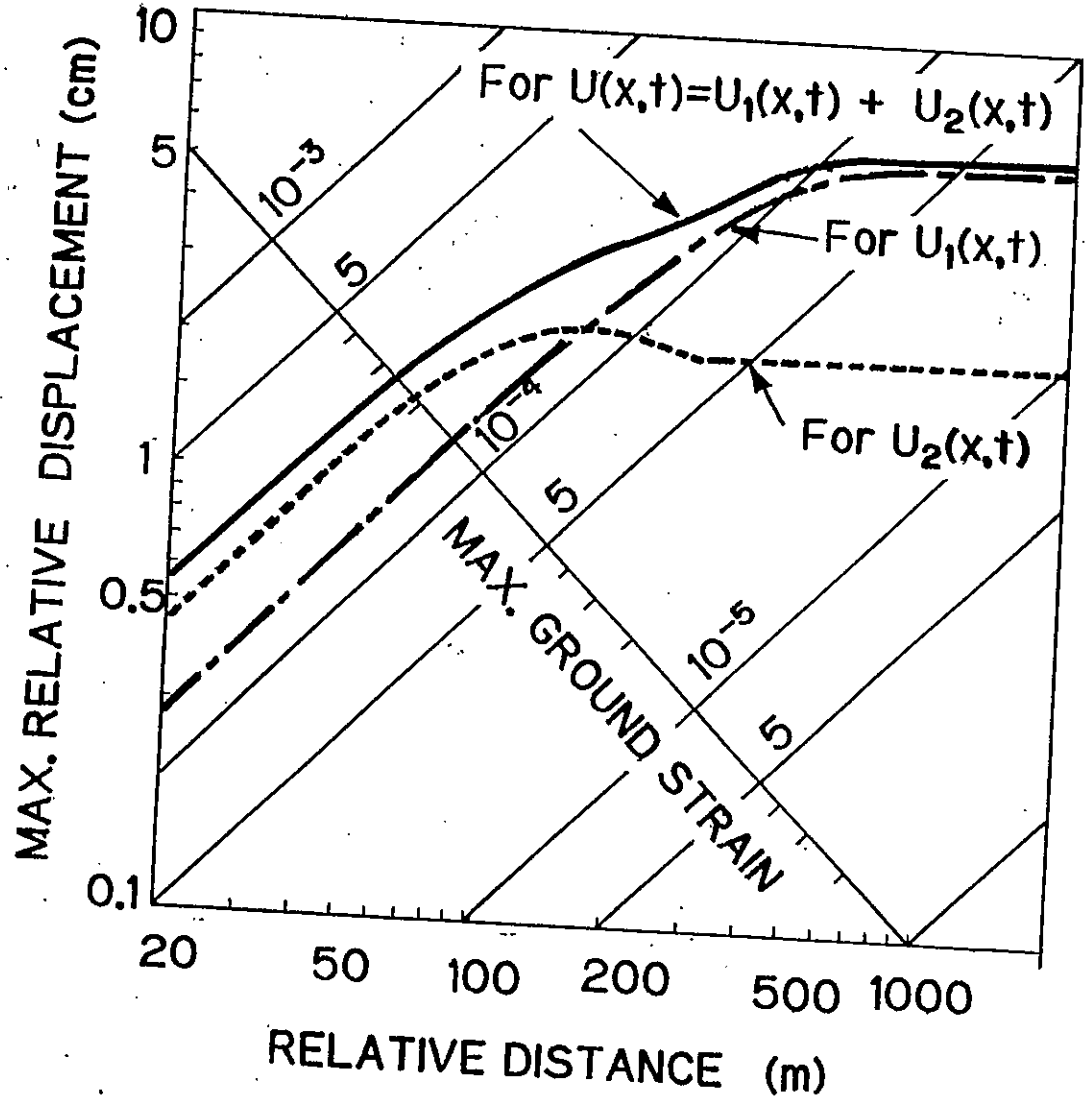

Fig. 6-6

Ground Deformation Spectra for Total Response Displacement $u(x,t)$ (Solid Curve) and for Response Displacements $u_1(x,t)$ and $u_2(x,t)$ (Dashed Curves)

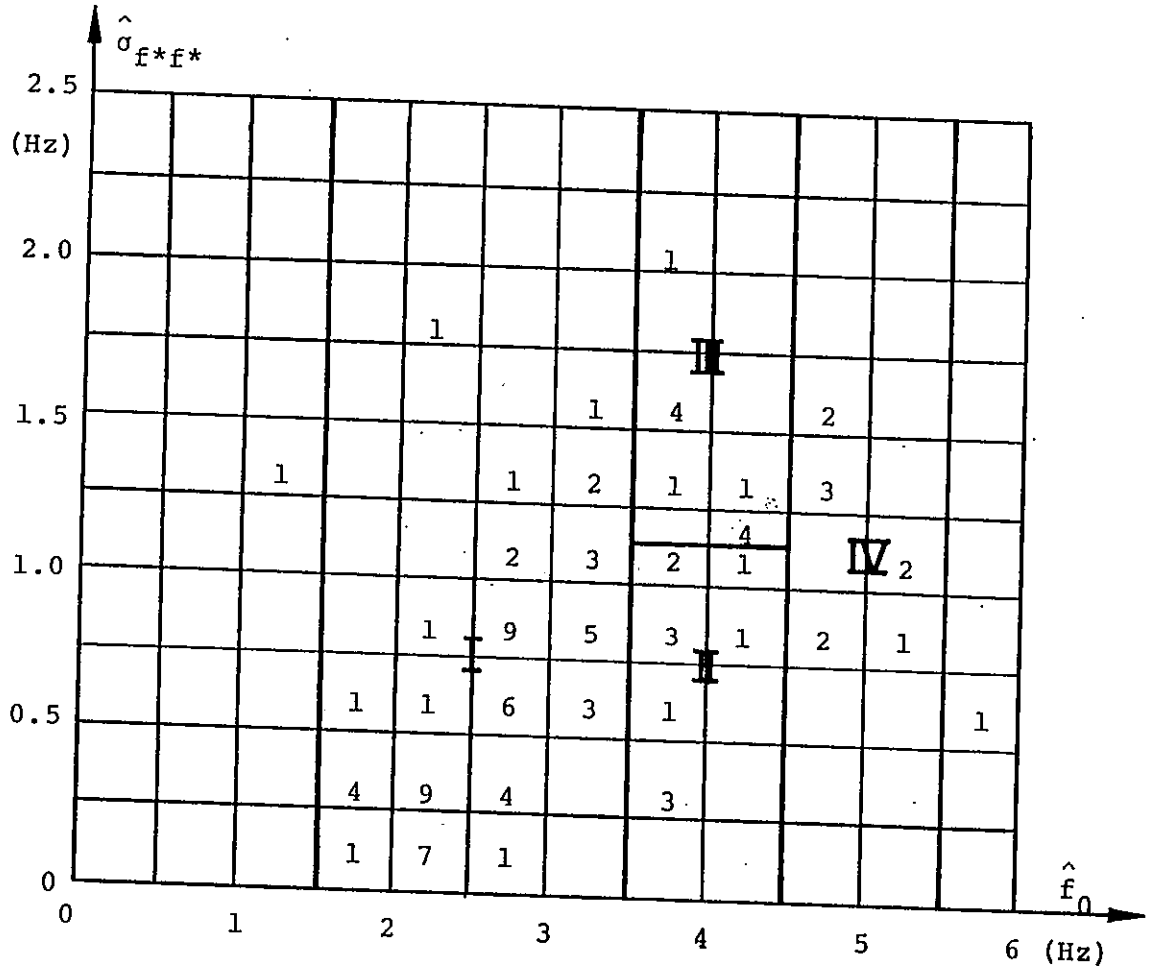

Fig. 7-1 Frequency Distribution of $\hat{f}_0 - \hat{\sigma}_{f^*f^*}$ Combinations

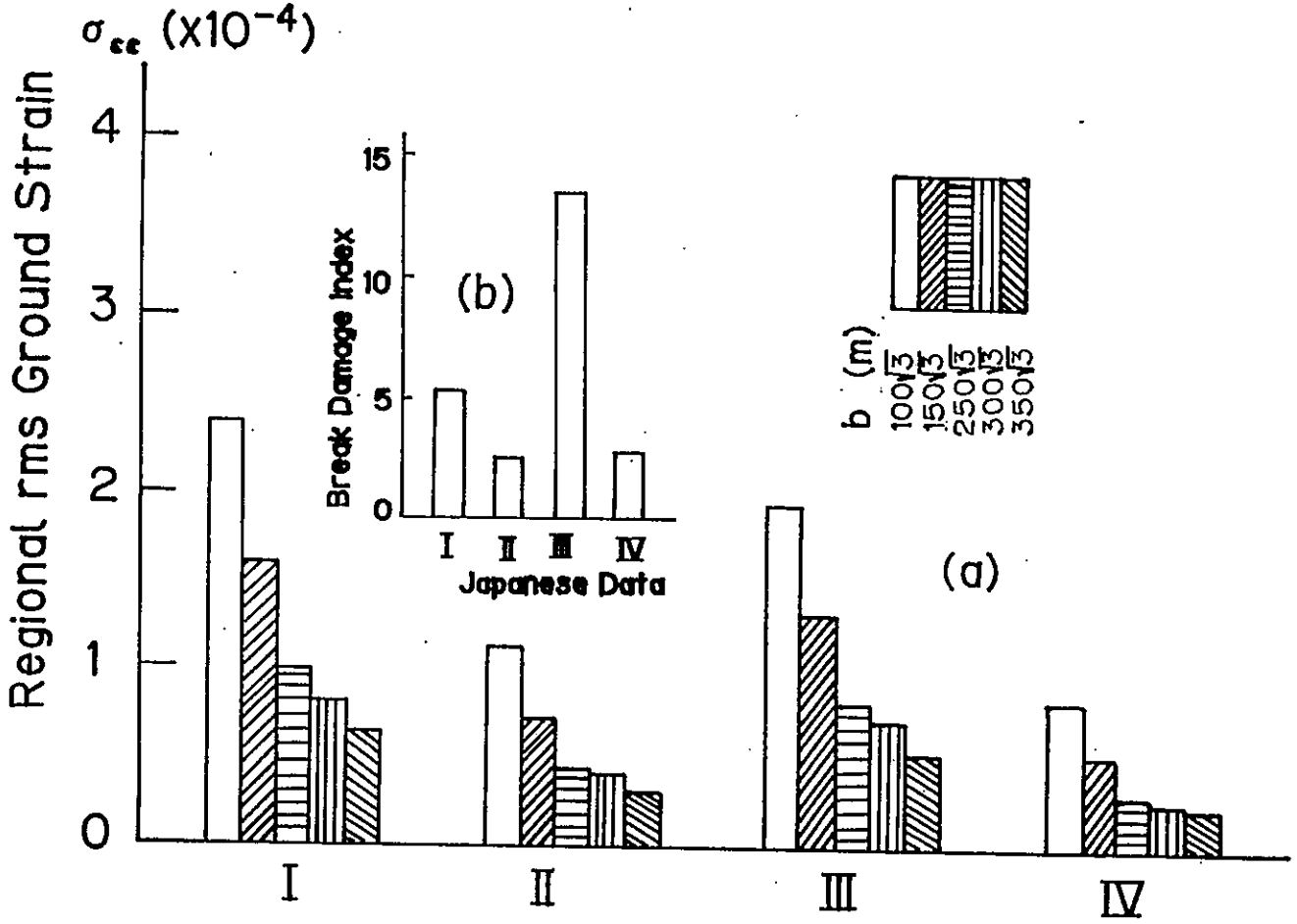

Fig. 7-2 Regional rms Ground Strains σ_{ee}
(Input Acc. = 200 cm/s^2, T = 10 sec, $\beta = 4/\pi$
$h_0 = 0.3$)

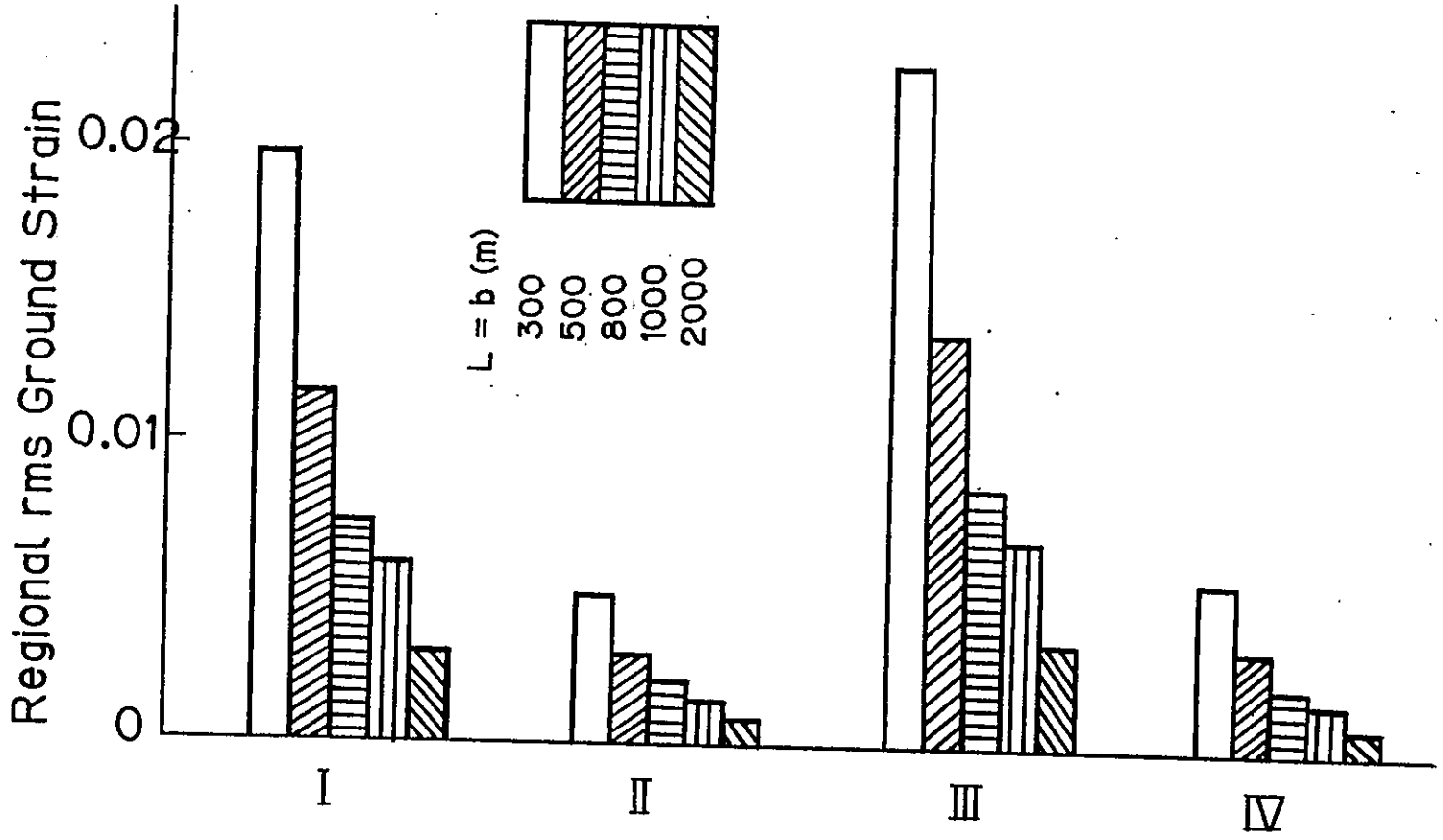

Fig. 7-3 Regional rms Ground Strain from Numerical Simulation (Shinozuka and Kawakami , 1977)

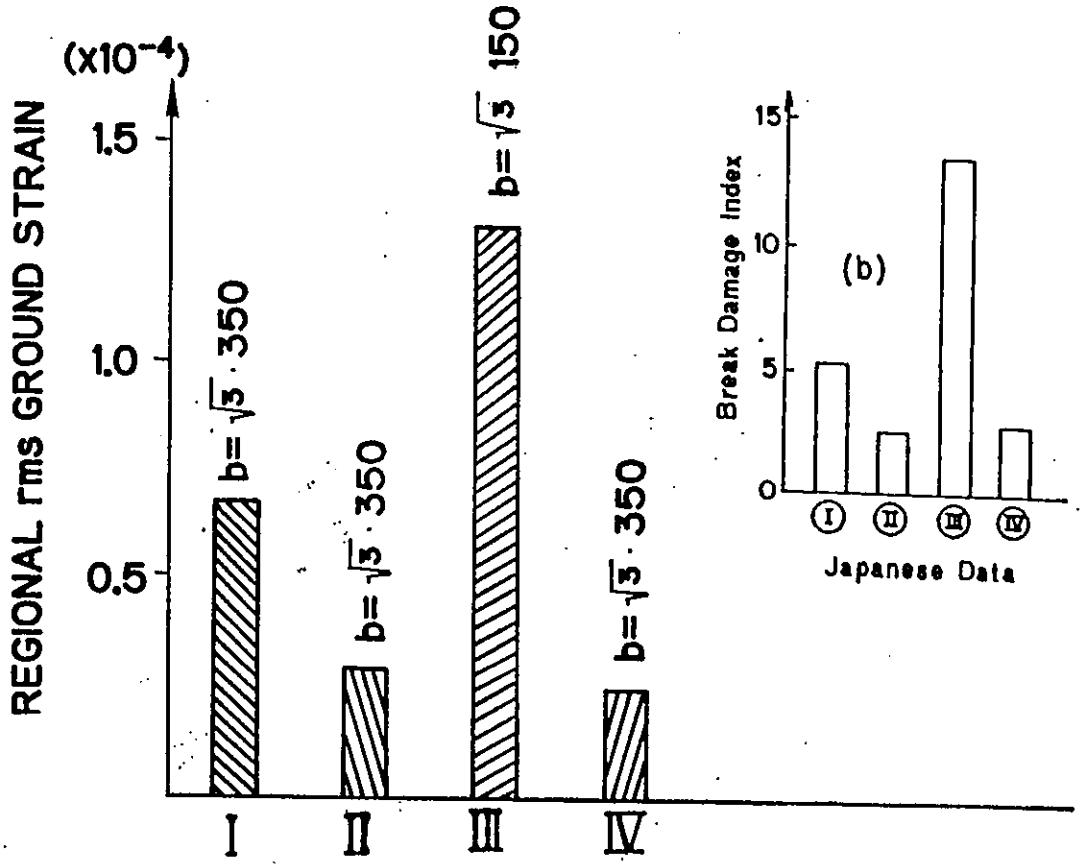

Fig. 7-4 Modified Regional rms Ground Strain $\sigma_{\varepsilon\varepsilon}$